Geometry dependent Reduced-Order Models for the computation of homogenized transfer properties in porous Media, Part II -Electrical Double Layer effects

Antoine Moreau, Cyrille Allery, Olivier Millet, Antoine Falaize

Acta Mechanica manuscript No.
(will be inserted by the editor)

Geometry dependent Reduced-Order Models for the computation of homogenized transfer properties in porous Media, Part II - Electrical Double Layer effects

Antoine Moreau · Cyrille Allery · Olivier Millet · Antoine Falaize

Received: date / Accepted: date

Abstract A Reduced-Order Model (ROM) based on Proper Orthogonal Decomposition (POD) is proposed to solve fastly the strongly nonlinear Elementary Cell Problem derived from the Periodic Homogenization of the Nernst-Planck-Poisson-Boltzmann equations. In previous works, multiscale models have been developed, in order to take separately into account the macro and microscopical aspects of ionic diffusion, under the assumption that the porous medium consists of the periodic repetition of a single microscopic Representative Elementary Volume (REV). More recently, a numerical method based on POD-ROM has been developed in order to take into account the variability of the REV at the macroscopical scale, which involves the numerical resolution of a large amount of instances of the Cell Problem. Presently, this method is extended to the case where the REV's size is of the order of the Debye Length and where the adsorption during the transfer of ions by the solid-fluid interface is considered.

Keywords: Homogenization, ionic diffusion, Debye length, Reduced Order Model, Proper Orthogonal Decomposition

1 Introduction

Early degradation of reinforced concrete buidings exposed to sea water is due to chloride diffusion in the pore solution. Indeed, chloride diffuse inside the water contained in the concrete's pores until they reach the steel skeleton. This induces oxidation-reduction and swelling of the rebar, threatening the whole structure. Thus, it is necessary to understand transfer mechanism in cementitious media and to model them precisely at a microscopical scale. Such a modelization is not possible at the scale of a whole structure, which motivates the use of homogenization techniques. Introduced by Whitaker [41,42] in the case of volume averaging methods, these consist of assimilating the porous medium to a virtual homogeneous medium, whose physical properties (here diffusion coefficients) are computed on microscopical elementary cells. Computational homogenization covers a wide range of numerical methods like the FE2 method introduced by Feyel in [16] which combines Finite Elements simulations at both macro- and micro- scales ; this method has been applied to the modelization of foams in [23]. Homogenization methods have also been applied to multiphysics modelization like in [14] where homogenization is combined to deep neural networks in the context of multiscale deformations. In this work we focus on periodic homogenization method [3, 37], applied to a problem that depends both on geometrical and physical parameters.

A. Moreau
E-mail: antoine.moreau@univ-lr.fr

C. Allery
E-mail: cyrille.allery@univ-lr.fr

O. Millet
E-mail: olivier.millet@univ-lr.fr

A. Falaize
E-mail: antoine.falaize@univ-lr.fr
LaSIE UMR-7356-CNRS, Université de La Rochelle Pôle Science et Technologie, Avenue Michel Crépeau 17042 La Rochelle Cedex 1, France

Usually, ionic diffusion in saturated porous media is modelled by Nernst-Planck-Poisson (NPP) equations, which combine Fick law, and transport of ions by electrical field in the pore solution. Furthermore, at the Debye lenght scale, ionic diffusion is influenced by the electrical double layer (EDL) of ions that have been adsorbed by the solid-fluid interface. According to the model proposed by Gouy and Chapman [21], that was used in [29,30,36] to model electrical double layers in clays, the EDL results in an electrical potential so that the pore solution close to the solid-fluid interface is not neutral. The ionic species concentrations are then determined by a Boltzmann factor, which in turn depends on the EDL potential. This model, combined to the NPP (electro-)diffusion equations, gives the Nernst-Planck-Poisson-Boltzmann equations for ionic diffusion at the EDL scale.

The periodic homogenization technique is relevant to obtain macroscopic models of ionic diffusion when applied to NPP or NPPB equations [9–11]. It assumes that microstructure of the porous medium is assimilated to the periodic repetition of an elementary cell which must be small enough comparatively to the whole medium size, in order to the macro and micro scales to be separated Homogenized properties, which are supposed not to vary at the macroscopical scale, are then computed by solving on the REV a partial differential equation called the cell problem. The resolution of the cell problem is generically done numerically. Then it remains to solve the Nernst-planck-Poisson equation at the maroscopical scale, provided homogenized coefficients, to simulate a diffusion process depending on time. This approach has been successfully used to model ionic transfer phenomenon in porous media [4,5,9], as well as other phenomenen like diffusion-advection-adsorption of pollutant in clays [1,2] and to diffusion reaction coupled problems [8,12,25,26].

However, in cementitious media, the REV geometry is complex, and varies over time. For the latter reason, a single REV may not be sufficient to represent the microstructure of a whole concrete structure. Thus, in order to use the periodic homogenization procedure, several REV must be considered, to take into account the variability of the microstructure and its possible time-dependent evolution. Then, for each REV, we must solve the cell problem (composed of several partial differential equations). The issue is that it is computationally expensive, especially because of nonlinearities. To overcome this difficulty it is possible to use a model order reduction approach to obtain in reduced time the diffusion properties when the geometry of the REV varies. A previous work [28] based on a ROM obtained by Proper Orthogonal Decomposition (POD) has been dedicated to the resolution of a great number of cell problems, depending on geometrical parameters, in the case of the NPP system, where the EDL effects are neglected. POD-ROM consists in, for a parametrized space dependent problem, structuring an orthonormal family of space-dependent functions, which are the most representative of the solution to the problem, for all parameter values considered. The original full-order problem is then projected on these spatial modes to obtain the reduced-order model (ROM) valid for each parameter, which allows to approximate the parameter dependent solutions in a lower dimensional subspace that retains mean features of the original full system. Thus, and contrarily to the Full-Order Model (FOM), the ROM is a set of algebraic equations whose size is reduced. The POD-ROM method is of current use in engineering sciences such as Fluid Mechanics [22,35], Fluid-Structure Interaction [15,27] and control problems [31,32] ... Performing POD for a geometry dependent problem is not straightforward, and the issue was adressed in [28] using a parametrized geometrical transformation linking the REVs to a reference elementary cell, on which POD was formulated. In the present work, the approach is generalized to the strongly non linear Nernst-Planck-Poisson-Boltzmann system. Several works also combine model order reduction methods to homogenization like in [44] for the modelization of hyperelastic media at finite strains, or in [23] where ROM is combined with the FE2 method, and more recently in [45] where POD contributes to the reduction of the number of variables that characterize damage at a microscopic scale. In [18], a reduced order homogenization method is presented in the case of materials including cohesive interfaces at microrcopic scale. Like in [44], this method relies on a single space coordinate system for the initial and the deformed state of a representative volume element, which corresponds to the undeformed state. However, this approach cannot be used for the geometry dependent ROMs seen in this work. In the present case, the NPP equation depends on the Boltzmann factor $r = e^{-B\varphi}$ associated with the electrical potential φ generated by the EDL. The latter is computed from the electrical potential, which is solution of the Poisson-Boltzmann equation (PB), which is strongly nonlinear and depends on the physical parameters of the EDL. The difficulty to apply POD-ROM here, is due to the fact that the Boltzmann factor is an exponential function of the potential φ solution of the PB equation (5). It seems natural and easy to build a ROM associated to the variable φ but it is not efficient in terms of computation time because of the nonlinearity of the Boltzmann factor, which would entail, at each use of the ROM, the expensive projection of the full-order problem on the POD basis of φ. To avoid this problem, it would be possible to use the Discrete Empirical Interpolation Method (DEIM) approach [13,43], combined with Finite Element Method. Here, we propose to apply directely the POD to the factor r which implies to reformulate the PB equation into a problem explicitely dependent on the Boltzmann factor r.

The aim of this paper is to propose a method to compute, in a reduced time, the homogenized coefficients derived from NPPB cell problems for a large number of REVs. It is organized as follows. In section 2, the

periodic homogenization of the multiscale ionic diffusion model is summarized and the classical cell problem is recalled. In section 3, the proposed POD based model order reduction method is presented. We firstly detail the procedure for an elementary cell with a single inclusion and secondly generalize it to the case of multiple inclusions. In section 4, we present numerical results that illustrate the accuracy and the reduced computational cost of the proposed method. Applications are done on a three-dimensional isotropic elementary cell depending on a single geometry parameter, for various values of physical parameters C_b and σ, and on a two-dimensional cell, with eight solid inclusions, depending themselves on two geometry parameters.

2 Problem statement

In this section, we firstly present the Nernst-planck-Poisson-Boltzmann (NPPB) equations which rule ionic diffusion in a saturated porous medium[1] like cementitious media, taking into account for the electrical double layer (EDL) due to adsorbed ion on the solid-fluid interface. Secondly, we recall briefly the periodic homogenization technique and present the results when it is applied to the NPPB system. In a third time, we explicit the calculation of the macroscopic homogenized coefficients from the ROM proposed for the non linear cell problem.

2.1 Ionic diffusion with EDL effect

Consider a saturated porous (cementitious) medium occupying a domain constituted of a path-wise connected fluid phase $\Omega_\mathrm{f} \subset \Omega$ through which ions can migrate, a solid phase $\Omega_\mathrm{s} = \Omega \setminus \Omega_\mathrm{f}$ (not necessarily path-wise connected), and a solid-fluid interface Γ_sf (see figure 1).

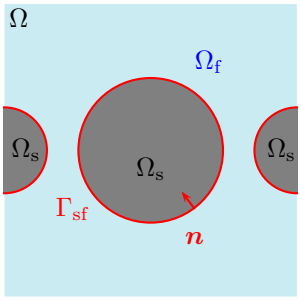

Fig. 1: Schematic view of a typical saturated porous medium, with fluid phase Ω_f, solid inclusions Ω_s and solid-fluid interface Γ_sf.

Ionic diffusion of anions and cations in the pore solution obeys the Nersnt-Planck equations:

$$\begin{cases} \dfrac{\partial c_\pm}{\partial t} - D_\pm \operatorname{div}\left(\nabla c_\pm \pm B\, c_\pm \nabla \Psi\right) = 0, & \text{in } \Omega_\mathrm{f}, \\ \left(\nabla c_\pm \pm B\, c_\pm \nabla \Psi\right) \cdot \boldsymbol{n} = 0, & \text{on } \Gamma_\mathrm{sf}, \end{cases} \tag{1}$$

where the $c_\pm$ (mol.m^{-3}) denote the concentrations of anions (c_-) and cations (c_+) in the pore solution, Ψ (V) the electrical potential, $D_\pm$ (m^2.s^{-1}) the self-diffusion coefficients assumed to be constant, $B = \frac{F}{RT}$ with T (K) the constant temperature, $F = 96485$ (Cb.mol^{-1}) the Faraday's constant and $R = 8.314$ (J.K.mol^{-1}) the perfect gas constant. The homogeneous Neumann boundary condition stands from the impermeability of the pores with $\boldsymbol{n}$ the unit normal vector on Γ_sf exterior to Ω_f. Equation (1) consists in the Fick's law with the transport of electrically charges ions by the electrical field $\epsilon_v \nabla \Psi$. For an acqueous solution composed of two ionic species, with single positive and negative charge respectively, the Poisson equation for the electrical potential reads:

$$\begin{cases} \epsilon_v \Delta \Psi + F\,(c_+ - c_-) = 0, & \text{in } \Omega_\mathrm{f}, , \\ \epsilon_v \nabla \Psi \cdot \boldsymbol{n} = \sigma, & \text{on } \Gamma_\mathrm{sf}\,. \end{cases} \tag{2}$$

[1] The interested reader will find more information in [10, 19, 20, 40].

where σ (C.m^{-2}) is the surface charge density on $\Gamma_{\rm sf}$ and ϵ_v (C.V^{-1}.m^{-1}) the electrical permittivity of the pore solution.

Classically, the electrical potential is decomposed into ([6,9,10]):

$$\Psi = \psi_{\rm b} + \varphi^2\,, \tag{3}$$

where $\psi_{\rm b}$ is the electrical potential in the bulk (the pore solution far from the solid-fluid interface), and φ the potential generated by the EDL effects. According to the Gouy and Chapman (1913) model [21], the ionic species lying in a diffuse layer close to the EDL follow the Boltzmann distribution:

$$c_\pm = C_{\rm b}\, e^{\mp B\,\varphi}\,, \tag{4}$$

where $C_{\rm b}$ is the ionic concentration in the bulk. Following equation (2) combined with relation (4) leads to the Poisson-Boltzmann equation:

$$\begin{cases} \epsilon_v \Delta\varphi - 2F\, C_{\rm b} \sinh\left(B\,\varphi\right) = 0, & \text{in } \Omega_{\rm f}, \\ \epsilon_v \nabla\varphi\cdot\boldsymbol{n} = \sigma, & \text{on } \Gamma_{\rm sf}, \end{cases} \tag{5}$$

which describes ionic diffusion at the microscopical scale. Resolution of this nonlinear, transcendental equation provides the electrical double layer potential φ.

2.2 Periodic homogenization

Periodic homogenization is based on the assumption that the porous medium with characteristic length L (m) can be well approximated by the periodic repetition of a single microscopic cell with characteristic length ℓ (m), representative of the real microstructure (see figure 2). In the sequel, we adopt the classical notation: $\boldsymbol{x}$ for the spatial coordinates at macroscopical scale, and $\boldsymbol{y}$ for spatial coordinates at the microscopical scale. Finally, the overall solid and fluid domain of the elementary cell Y will be noted $\rm Y_s$ and $\rm Y_f$, and its solid-fluid interface will be noted $\rm S_{sf}$.

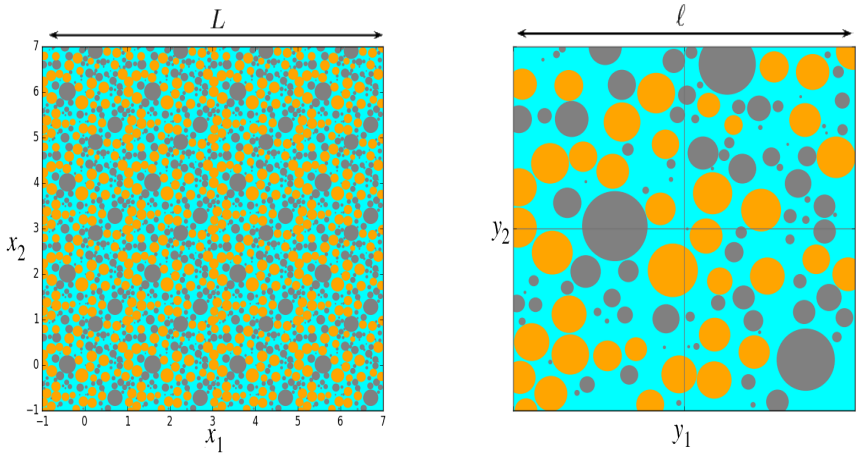

(a) Periodic microstructure (b) Elementary Cell or REV

Fig. 2: Example of a periodic microstructure

Provided the relation

$$\epsilon = \frac{\ell}{L} \ll 1\,, \tag{6}$$

which is a homogenizability condition, the periodic homogenization procedure [6,7,9,10] consists in developping the physical quantities $c_\pm$, Ψ, φ as formal power series of the perturbation parameter $\epsilon = \dfrac{\ell}{L}$

[2] This relation is the electroneutrality of the system constituted of the pore space and the interface.

$$c_\pm = {c_\pm}^0(\boldsymbol{x},\boldsymbol{y},t) + \epsilon {c_\pm}^1(\boldsymbol{x},\boldsymbol{y},t) + \epsilon^2 {c_\pm}^2(\boldsymbol{x},\boldsymbol{y},t) + \dots , \tag{7}$$

$$\psi_\mathrm{b} = {\psi_\mathrm{b}}^0(\boldsymbol{x},\boldsymbol{y},t) + \epsilon {\psi_\mathrm{b}}^1(\boldsymbol{x},\boldsymbol{y},t) + \epsilon^2 {\psi_\mathrm{b}}^2(\boldsymbol{x},\boldsymbol{y},t) + \dots , \tag{8}$$

$$\varphi = \varphi^0(\boldsymbol{x},\boldsymbol{y},t) + \epsilon \varphi^1(\boldsymbol{x},\boldsymbol{y},t) + \epsilon^2 \varphi^2(\boldsymbol{x},\boldsymbol{y},t) + \dots , \tag{9}$$

whose terms before ϵ^0, ϵ^1, ϵ^2 ... represent the physical quantities of NPPB equations at different space scales.

The leading term (C_b^0, φ^0) in the NPPB equations is then identified through the resulting cascading problems coming from the cancellation of powers in ϵ^p, $p \in \mathbb{Z}$. It is solution of the expected homogenized problem (see [6, 7, 9, 10] for more details) summarized below where C_b^0 and φ^0 have been denoted C_b and φ for ease of reading

$$\varepsilon_\mathbf{p} \frac{\partial \langle C_\mathrm{b} e^{\mp B\varphi} \rangle_{\boldsymbol{y}}}{\partial t} - \operatorname{div}_{\boldsymbol{x}} \left(\boldsymbol{D}_\pm^\mathrm{hom} \left(\nabla_{\boldsymbol{x}} C_\mathrm{b} \pm B\, C_\mathrm{b} \nabla_{\boldsymbol{x}} \psi_\mathrm{b} \right) \right) = 0 \tag{10}$$

where $\langle\ \rangle_{\boldsymbol{y}}$ is the spatial mean-value operator on the Elementary Cell fluid domain. $\varepsilon_\mathbf{p}$ denotes the medium's porosity defined by $\varepsilon_\mathbf{p} = \dfrac{|\mathrm{Y_f}|}{|\mathrm{Y}|}$ with $|\mathrm{Y}|$ the volume of Y. The homogenized diffusion tensor is given by:

$$\boldsymbol{D}_\pm^\mathrm{hom} = \frac{1}{|\mathrm{Y}|} \int_{\mathrm{Y_f}} D_\pm\, e^{\mp B\,\varphi} \left(\boldsymbol{I} + \nabla_{\boldsymbol{y}}^\intercal \boldsymbol{\chi}_\pm \right) \mathrm{d}\mathrm{Y} , \tag{11}$$

where $\boldsymbol{A}^\intercal$ denotes the transposition operator of tensor $\boldsymbol{A}$.

Electrical potential φ, at the microscale, is solution of:

$$\begin{cases} \epsilon_v \Delta_{\boldsymbol{y}} \varphi = 2\, F\, C_\mathrm{b} \sinh\left(B\,\varphi\right) & \text{in } \mathrm{Y_f}, \\ \epsilon_v\, \nabla_{\boldsymbol{y}} \varphi \cdot \boldsymbol{n} = \sigma & \text{on } \mathrm{S_{sf}}\,. \end{cases} \tag{12}$$

Moreover, vector field $\boldsymbol{\chi}_\pm$ is solution to the following equation:

$$\begin{cases} \operatorname{div}_{\boldsymbol{y}} \left(D_\pm\, e^{\mp B\,\varphi} \left(\boldsymbol{I} + \nabla_{\boldsymbol{y}} {\boldsymbol{\chi}_\pm}^\intercal \right) \right) = 0 & \text{in } \mathrm{Y_f}, \\ \left(D_\pm\, e^{\mp B\,\varphi} \left(\boldsymbol{I} + \nabla_{\boldsymbol{y}} \boldsymbol{\chi}_\pm \right) \right) \cdot \boldsymbol{n} = \boldsymbol{0} & \text{on } \mathrm{S_{sf}}, \end{cases} \tag{13}$$

The problem (13) where φ is given by (12) constitutes the so-called cell problem, whose solutions characterize geometrical and physical properties of the REV. Since the two problems are analogous, and for the sake of simplicity, we will only consider this multiscale model for a single, positively charged ionic specy. Thus we drop the $\pm$ specification from all quantities in the sequel. Furthermore, the ionic diffusion coefficient D in the pore solution is assumed to be constant.

2.3 Reduced Order Model for the NPPB equations

2.3.1 A geometry dependent reduced order model

The aim of this work is to compute fastly the homogenized tensor $\boldsymbol{D}^\mathrm{hom}$ given by (11) for an elementary cell whose geometry depends on a vector set of parameters $\boldsymbol{\rho}$. We can for example take the Elementary Cell figured on Fig. 2b, and choose for parameters the radii $\rho_1, \dots, \rho_n$ of its solid inclusions. A fast computation of $\boldsymbol{D}^\mathrm{hom}$ for each individual value of $\boldsymbol{\rho}$ is useful if one needs to take care of the variability of a porous medium geometry. The approach consists in approximating the vector field $\boldsymbol{\chi}$ and the electrical double layer potential φ into the following form:

$$\widehat{\boldsymbol{\chi}}(\boldsymbol{y},\boldsymbol{\rho}) \simeq \sum_{j=1}^{n_{\boldsymbol{\chi}}} a_j(\boldsymbol{\rho})\, \boldsymbol{\phi}_j(\boldsymbol{y}) \quad \text{and} \quad \widehat{\varphi}(\boldsymbol{y},\boldsymbol{\rho}) \simeq \sum_{i=1}^{n_\varphi} p_i(\boldsymbol{\rho})\, \phi_i^\varphi(\boldsymbol{y}) , \tag{14}$$

where $(\boldsymbol{\phi}_j)_j$ and $(\phi_i^\varphi)_i$ are two sets of orthogonal space-dependent functions, that will be used to perform the Galerkin projection of the associated weak form of the cell problem (see appendix A).

In a previous work [28], for the case of NP problem where the EDL effects are neglected (that corresponds to $e^{-B\sum_{i=1}^{n_\varphi} p_i(\boldsymbol{\rho})\phi_i^\varphi(\boldsymbol{y})} \simeq 1$), the authors used an efficient POD-ROM in which explicitely appears the geometrical parameters $\boldsymbol{\rho} = (\rho_1, \ldots, \rho_n)$. It is based on an analytical transformation which maps the various geometrical domains $\mathrm{Y_f}(\boldsymbol{\rho})$ on a reference domain $\mathrm{Y_f^\star} = \mathrm{Y_f}(\boldsymbol{\rho}_\star)$. In the present paper, the method is extended to the NPPB problem. Now we present the approach for the NPPB problem.

2.3.2 Recall on the correlations tensors

Coefficients $a_j(\boldsymbol{\rho})$ and $p_i(\boldsymbol{\rho})$ are obtained by solving a set of algebraic equations whose size is of the order of $n_{\boldsymbol{\chi}}$, the so-called reduced-order model (ROM). The spatial functions or modes $\boldsymbol{\phi}_j$ and ϕ_i^φ are built using Proper Orthogonal Decomposition (POD) with the method of snapshots [39]. More precisely, the so-called Snapshot POD for field $\boldsymbol{\chi}$ or φ consists of computing, for a finite set $\boldsymbol{\rho}_1,\ \boldsymbol{\rho}_2,\ \ldots\ ,\ \boldsymbol{\rho}_{n_{\mathrm{snap}}}$ of values of the geometry parameter, particular solutions of the cell problems (12)–(13), using the classical, Finite Element Method. Once these solutions have been computed, the spatial correlation tensors

$$[\boldsymbol{C}^\varphi]_{ij} = \int_{\mathrm{Y_f}} \varphi(\boldsymbol{y},\boldsymbol{\rho}_i)\varphi(\boldsymbol{y},\boldsymbol{\rho}_j)\,\mathrm{dY} \quad \text{and} \quad [\boldsymbol{C}^{\boldsymbol{\chi}}]_{ij} = \int_{\mathrm{Y_f}} \boldsymbol{\chi}(\boldsymbol{y},\boldsymbol{\rho}_i)\cdot\boldsymbol{\chi}(\boldsymbol{y},\boldsymbol{\rho}_j)\,\mathrm{dY} \tag{15}$$

are computed. Their eigenvalues and eigenvectors provide the POD spatial modes ϕ_i^φ and $\boldsymbol{\phi}_j$. In both expressions in (15), a unique integration (fluid) domain $\mathrm{Y_f}$ is needed, which is not possible if $\boldsymbol{\rho}_i \neq \boldsymbol{\rho}_j$. This motivates the reformulation of the cell problems on a single geometrical domain $\mathrm{Y}^\star$ with spatial coordinates $\boldsymbol{\xi}$, where the dependency on the geometrical parameter $\boldsymbol{\rho}$ lies in Jacobian matrices $\widehat{\boldsymbol{J}_{\boldsymbol{\rho}}}$ (respectively its determinant $\widehat{j_{\boldsymbol{\rho}}}$), which are tensor fields (respectively scalar fields). The transformation that maps $\mathrm{Y_f}$ to $\mathrm{Y_f^\star}$ that has been proposed in [28] is detailed in appendix B.2.

2.3.3 The POD-ROM for NPPB and Poisson-Boltzmann: Galerkin projection

Taking the EDL into account for periodic homogenization leads to the weak form of the Nernst-Planck-Poisson-Boltzmann problem (13):

$$\int_{\mathrm{Y_f}} e^{-B\varphi}\nabla_{\boldsymbol{y}}\boldsymbol{\chi}\colon\nabla_{\boldsymbol{y}}\boldsymbol{v}\mathrm{dY} = \int_{\mathrm{Y_f}} \nabla_{\boldsymbol{y}}\left(e^{-B\varphi}\right)\cdot\boldsymbol{v}\mathrm{dY} - \int_{\mathrm{S_{sf}}} e^{-B\varphi}\boldsymbol{v}\cdot\boldsymbol{n}\mathrm{dS} \quad \forall\boldsymbol{v}\in V_\rho\,, \tag{16}$$

where V_ρ is the space of regular vector-valued functions defined on $\mathrm{Y_f}$.

After a pullback[3] $\boldsymbol{\xi} = \widehat{\boldsymbol{\tau}_{\boldsymbol{\rho}}}^{-1}\boldsymbol{y}$ on the reference domain $\mathrm{Y}^\star$, it may rewritten as

$$\int_{\mathrm{Y_f^\star}} e^{-B\varphi_\star}\left(\nabla_{\boldsymbol{\xi}}\boldsymbol{\chi}_\star\,\widehat{\boldsymbol{J}_{\boldsymbol{\rho}}}^{-1}\right)\colon\left(\nabla_{\boldsymbol{\xi}}\boldsymbol{v}_\star\,\widehat{\boldsymbol{J}_{\boldsymbol{\rho}}}^{-1}\right)\widehat{j_{\boldsymbol{\rho}}}\mathrm{dY}^\star = \int_{\mathrm{Y_f^\star}} \widehat{\boldsymbol{J}_{\boldsymbol{\rho}}}^{-\intercal}\nabla_{\boldsymbol{\xi}}\, e^{-B\varphi_\star}\cdot\boldsymbol{v}_\star\,\widehat{j_{\boldsymbol{\rho}}}\mathrm{dY}^\star - \int_{\mathrm{S_{sf}}^\star} e^{-B\varphi_\star}\boldsymbol{v}_\star\cdot\boldsymbol{n}_\star\, g_{\boldsymbol{\rho}}\,\mathrm{dS}^\star \quad \forall\boldsymbol{v}_\star\in V_\star, \tag{17}$$

where

$$\boldsymbol{\chi}_\star(\boldsymbol{\xi},\boldsymbol{\rho}) = \boldsymbol{\chi}(\boldsymbol{y},\boldsymbol{\rho}), \tag{18}$$
$$\varphi_\star(\boldsymbol{\xi},\boldsymbol{\rho}) = \varphi(\boldsymbol{y},\boldsymbol{\rho}), \tag{19}$$
$$\boldsymbol{v}_\star(\boldsymbol{\xi},\boldsymbol{\rho}) = \boldsymbol{v}(\boldsymbol{y},\boldsymbol{\rho}). \tag{20}$$

and where $V_\star$ is the space of vector-valued functions defined on $\mathrm{Y_f^\star}$.

Moreover, relation (11) becomes

$$\boldsymbol{D}^{\mathrm{hom}} = \frac{1}{|\mathrm{Y}^\star|}\int_{\mathrm{Y_f^\star}} D\, e^{-B\varphi_\star}\left(\boldsymbol{I} + \nabla_{\boldsymbol{\xi}}\boldsymbol{\chi}_\star\,\widehat{\boldsymbol{J}_{\boldsymbol{\rho}}}^{-1\intercal}\right)\widehat{j_{\boldsymbol{\rho}}}\,\mathrm{dY}^\star, \tag{21}$$

Once the POD basis is obtained, approximations (14) are substituted in equation (17). Thus, the ROM is obtained:

[3] See the previous work [28] or Appendix B.1 for a detailed presentation

$$\int_{\mathrm{Y_f^\star}} e^{-B\sum_{i=1}^{n^\varphi} p_i(\boldsymbol{\rho})\phi_i^\varphi} \nabla\Big(\sum_{j=1}^{n_{\boldsymbol{\chi}}} a_j(\boldsymbol{\rho})\,\boldsymbol{\phi}_j\Big)\,\widehat{\boldsymbol{J}_{\boldsymbol{\rho}}}^{-1} : \nabla\boldsymbol{\phi}_l\,\widehat{\boldsymbol{J}_{\boldsymbol{\rho}}}^{-1}\,\widehat{j_{\boldsymbol{\rho}}}\,\mathrm{dY}^\star = \int_{\mathrm{Y_f^\star}} \widehat{\boldsymbol{J}_{\boldsymbol{\rho}}}^{-\mathsf{T}} \left(\nabla e^{-B\sum_{i=1}^{n^\varphi} p_i(\boldsymbol{\rho})\phi_i^\varphi}\right)\cdot\boldsymbol{\phi}_l\,\widehat{j_{\boldsymbol{\rho}}}\,\mathrm{dY}^\star$$
$$- \int_{\mathrm{S_{sf}}^\star} e^{-B\sum_{i=1}^{n^\varphi} p_i(\boldsymbol{\rho})\phi_i^\varphi}\,(\boldsymbol{\phi}_l\cdot\boldsymbol{n}_\star)\,\widehat{j_{\boldsymbol{\rho}}}\,\mathrm{dS}^\star \quad \forall l\in 1,\dots,n_{\boldsymbol{\chi}} \tag{22}$$

and the same operation on (21) gives (see also [28] for more details)

$$\boldsymbol{D}^{\mathrm{hom}} = \frac{1}{|\mathrm{Y}^\star|}\int_{\mathrm{Y_f^\star}} D\,e^{-B\sum_{i=1}^{n^\varphi} p_i(\boldsymbol{\rho})\phi_i^\varphi}\left(\boldsymbol{I} + \left(\nabla\Big(\sum_{j=1}^{n_{\boldsymbol{\chi}}} a_j(\boldsymbol{\rho})\,\boldsymbol{\phi}_j\Big)\,\widehat{\boldsymbol{J}_{\boldsymbol{\rho}}}^{-1}\right)^{\mathsf{T}}\right)\widehat{j_{\boldsymbol{\rho}}}\,\mathrm{dY}^\star\,. \tag{23}$$

In expressions (22)-(23), the sum $\sum_{j=1}^{n_{\boldsymbol{\chi}}}$ and integral symbols can be inverted, but this is not the case of the symbols $\int$ and $\sum_{i=1}^{n^\varphi}$, due to the nonlinearity of the factor

$$e^{-B\sum_{i=1}^{n^\varphi} p_i(\boldsymbol{\rho})\phi_i^\varphi(\boldsymbol{\xi})}\,. \tag{24}$$

Consequently, every expression in (22)–(23) involving the factor (24) must be integrated for each value of $\boldsymbol{\rho}$ in order to perform the Galerkin projection. As these integral computations cannot be done in a reduced time, the ROM efficiency is compromised.

Obviously, the same difficulty is encountered when performing model order reduction on the highly nonlinear, Poisson-Boltzmann equation (5). Both issues are adressed in the next section.

3 POD-ROM for NPPB

In this section, we present a POD reduced-order model dedicated to the computation, in a reduced time, of the homogenized tensor $\boldsymbol{D}^{\mathrm{hom}}$ which appears in the periodic homogenization procedure, in the case when Electrical Double Layer effects are taken into account. This reduced-order model relies on the reformulation of cell problems on a reference geometrical domain, using the method developed by the authors in [28]. Furthermore, the issues about Galerkin projection that have been outlined in the former section are resolved.

The main idea of this work is to rewrite the Poisson-Boltzmann equation (5) and the cell problem (13) as equations satisfied by the Boltzmann factor

$$r \overset{\mathrm{def}}{=} e^{-B\varphi}\,, \tag{25}$$

associated to the double layer potential φ. As well as for φ, r is pulled back onto the reference domain $\mathrm{Y_f^\star}$, and it results in the field $r_\star$ which verifies:

$$r_\star \overset{\mathrm{def}}{=} e^{-B\varphi_\star}\,, \tag{26}$$

where $\varphi_\star$ is defined by relation (19).

Let us write the POD of the field $r_\star$:

$$\widehat{r}_\star(\boldsymbol{\xi},\boldsymbol{\rho}) = \sum_{i=1}^{n_r} b_i(\boldsymbol{\rho})\,\phi_i^r(\boldsymbol{\xi})\,. \tag{27}$$

Thus, substituting $r_\star$ to $e^{-B\varphi_\star}$ in equation (17), the following equation is obtained

$$\int_{\mathrm{Y_f^\star}} r_\star\big(\nabla_{\boldsymbol{\xi}}\boldsymbol{\chi}_\star\,\widehat{\boldsymbol{J}_{\boldsymbol{\rho}}}^{-1}\big) : \big(\nabla_{\boldsymbol{\xi}}\boldsymbol{v}_\star\,\widehat{\boldsymbol{J}_{\boldsymbol{\rho}}}^{-1}\big)\,\widehat{j_{\boldsymbol{\rho}}}\mathrm{dY}^\star = \int_{\mathrm{Y_f^\star}} \widehat{\boldsymbol{J}_{\boldsymbol{\rho}}}^{-\mathsf{T}}\nabla_{\boldsymbol{\xi}}\,r_\star\cdot\boldsymbol{v}_\star\,\widehat{j_{\boldsymbol{\rho}}}\mathrm{dY}^\star - \int_{\mathrm{S_{sf}}^\star} r_\star\boldsymbol{v}_\star\cdot\boldsymbol{n}_\star\,g_{\boldsymbol{\rho}}\,\mathrm{dS}^\star \quad \forall\boldsymbol{v}_\star\in V_\star, \tag{28}$$

and it is possible to decompose the fields $\boldsymbol{\chi}_\star$, $\boldsymbol{v}_\star$, $r_\star$ on the two POD basis $(\phi_i^r(\boldsymbol{\xi}))_{i=1}^{n_r}$ and $(\boldsymbol{\phi}_j(\boldsymbol{\xi}))_{j=1}^{n_{\boldsymbol{\chi}}}$. This provides the reduced-order linear system whose solution is $(a_j(\boldsymbol{\rho}))_{j=1}^{n_{\boldsymbol{\chi}}}$

$$\sum_{j=1}^{n_{\boldsymbol{\chi}}} a_j(\boldsymbol{\rho}) \sum_{i=1}^{n_r} b_i(\boldsymbol{\rho}) \int_{\mathrm{Y}_\mathrm{f}^\star} \phi_i^r \, \nabla \, \boldsymbol{\phi}_j \, \widehat{\boldsymbol{J}_{\boldsymbol{\rho}}}^{-1} : \nabla \boldsymbol{\phi}_l \, \widehat{\boldsymbol{J}_{\boldsymbol{\rho}}}^{-1} \, \widehat{j_{\boldsymbol{\rho}}} \, \mathrm{dY}^\star = \sum_{i=1}^{n_r} b_i(\boldsymbol{\rho}) \int_{\mathrm{Y}_\mathrm{f}^\star} \widehat{\boldsymbol{J}_{\boldsymbol{\rho}}}^{-\intercal} \nabla \phi_i^r \cdot \boldsymbol{\phi}_l \, \widehat{j_{\boldsymbol{\rho}}} \, \mathrm{dY}^\star - \sum_{i=1}^{n_r} b_i(\boldsymbol{\rho}) \int_{\mathrm{S}_{\mathrm{sf}}{}^\star} \phi_i^r \, \boldsymbol{\phi}_l \cdot \boldsymbol{n}_\star \, g_{\boldsymbol{\rho}} \, \mathrm{dS}^\star \quad \forall l \in 1, \dots n_{\boldsymbol{\chi}} \,, \tag{29}$$

as well as the estimation of $\widehat{\boldsymbol{D}}^{\mathrm{hom}}$

$$\widehat{\boldsymbol{D}}^{\mathrm{hom}}(\boldsymbol{\rho}) = \frac{D}{|\mathrm{Y}^\star|} \left(\sum_{i=1}^{n_r} b_i(\boldsymbol{\rho}) \int_{\mathrm{Y}_\mathrm{f}^\star} \phi_i^r \, \widehat{j_{\boldsymbol{\rho}}} \, \mathrm{dY}^\star \right) \boldsymbol{I} + \frac{D}{|\mathrm{Y}^\star|} \sum_{j=1}^{n_{\boldsymbol{\chi}}} a_j(\boldsymbol{\rho}) \sum_{i=1}^{n_r} b_i(\boldsymbol{\rho}) \int_{\mathrm{Y}_\mathrm{f}^\star} \phi_i^r \left(\nabla_{\boldsymbol{\xi}} \, \boldsymbol{\phi}_j \, \widehat{\boldsymbol{J}_{\boldsymbol{\rho}}}^{-1} \right)^\intercal \widehat{j_{\boldsymbol{\rho}}} \, \mathrm{dY}^\star \,, \tag{30}$$

which is obtained by substituting $\widehat{r}_\star(\boldsymbol{\xi}, \boldsymbol{\rho}) = \sum_{i=1}^{n_r} b_i(\boldsymbol{\rho}) \, \phi_i^r(\boldsymbol{\xi})$ to $e^{-B \sum_{i=1}^{n^\varphi} p_i(\boldsymbol{\rho}) \phi_i^\varphi(\boldsymbol{\xi})}$ in relation (23). Contrarily to the ROMs of (22)–(23), which relied on the POD of the potential $\varphi_\star$, the inversion of operators $\sum_{i=1}^{n_r}$ and $\int$ is possible, providing the precomputation of the ROM coefficients.

The reformulation, involving $r = e^{-B\varphi}$, of the NPPB problem, followed by its model order reduction, consists in three steps:

1. Writing weak forms of the Poisson-Boltzmann equation involving the Boltzmann factor $r = e^{-B\varphi}$. These must depend multilinearily from r so that the Galerkin projection can be precomputed ;
2. Using the Galerkin projection, building a reduced-order model of the Poisson-Boltzmann equation that computes in a reduced time an estimate $\widehat{r}_\star$ of the Boltzmann factor ;
3. Using the Galerkin projection, building a reduced-order model that computes in a reduced time estimates $\widehat{\boldsymbol{\chi}}_\star$ (respectively $\widehat{\boldsymbol{D}}^{\mathrm{hom}}$) of the cell problem's solution (respectively of the diffusion tensor).

3.1 Reformulation of the Poisson-Boltzmann equation

Let us recall the strong formulation of Poisson-Boltzmann equation (5) on the elementary cell:

$$\begin{cases} \epsilon_v \Delta_{\boldsymbol{y}} \varphi - 2F \, C_\mathrm{b} \sinh\left(B \, \varphi\right) = 0, & \text{in } \mathrm{Y_f}, \\ \epsilon_v \nabla_{\boldsymbol{y}} \varphi \cdot \boldsymbol{n} = \sigma, & \text{on } \mathrm{S_{sf}}. \end{cases} \tag{31}$$

A weak form of this problem is derived using the divergence theorem on $\mathrm{Y_f} \cup \mathrm{S_{sf}}$:

$$\epsilon_v \int_{\mathrm{Y_f}} \nabla\varphi \nabla q \mathrm{dY} + 2F \, C_\mathrm{b} \int_{\mathrm{Y_f}} \sinh\left(B \, \varphi\right) q \mathrm{dY} = \int_{\mathrm{S_{sf}}} \sigma q \mathrm{dS} \,, \tag{32}$$

for all test function q in a function space $W_{\boldsymbol{\rho}}$ defined on the fluid domain $\mathrm{Y_f}$. By using the identities

- $\nabla\varphi = -B^{-1} r^{-1} \nabla r$,
- $\Delta\varphi = B^{-1} \left(\dfrac{\nabla r \cdot \nabla r}{r^2} - \dfrac{\Delta r}{r} \right)$,

associated to the Boltzmann factor r, it is seen that equation (31) is equivalent to

$$\begin{cases} \epsilon_v \left(r \Delta r - \nabla r \cdot \nabla r \right) = F \, B C_\mathrm{b} \left(r^3 - r \right) & \text{on } \mathrm{Y_f}, \\ \epsilon_v \nabla r \cdot \boldsymbol{n} = -Br\sigma & \text{on } \mathrm{S_{sf}}, \end{cases} \tag{33}$$

and (32) can be reformulated as

$$\epsilon_v \int_{\mathrm{Y_f}(\boldsymbol{\rho})} r^{-1} \nabla r \nabla q \mathrm{d}\Omega + F \, B C_\mathrm{b} \int_{\mathrm{Y_f}(\boldsymbol{\rho})} \left(-r^{-1} + r \right) q \mathrm{d}\Omega + B \int_{\mathrm{S_{sf}}(\boldsymbol{\rho})} \sigma q \mathrm{d}\Gamma = 0 \,, \forall q \in W_{\boldsymbol{\rho}} \,. \tag{34}$$

It must be noticed that, like in the case of the original Poisson-Boltzmann equation, it is not possible to precompute the coefficients of the ROM associated to equation (34). Indeed, if we write

$$\widehat{r}_\star = \sum_{i=1}^{n_r} b_i(\boldsymbol{\rho})\, \phi_i^r(\boldsymbol{\xi})\,, \tag{35}$$

and substitute the right side of (35) to r in equation (34), we see that the expression $\left(\sum_{i=1}^{n_r} b_i(\boldsymbol{\rho})\, \phi_i^r(\boldsymbol{\xi})\right)^{-1}$ appears in place of r^{-1}. Then, the sum $\sum_{i=1}^{n_r}$ and integral symbols in (34) can't be inverted, and the coefficients of the ROM must be computed for each parameter $\boldsymbol{\rho}$ where the ROM is supposed to be performed.

This issue is overcome by splitting equation (34) into a system of two equations, satisfied by a pair $(r,\, u)$ of scalar functions:

$$\begin{cases} \epsilon_v \displaystyle\int_{\mathrm{Y_f}} u\, \nabla r \cdot \nabla q \,\mathrm{dY} + C_\mathrm{b} B \int_{\mathrm{Y_f}} rq \,\mathrm{dY} = C_\mathrm{b} B \int_{\mathrm{Y_f}} uq \,\mathrm{dY} \;-\; B \int_{\mathrm{S_{sf}}} \sigma q \,\mathrm{dS}\,, \;\; \forall q \in W_{\boldsymbol{\rho}}\,, \\ ru = 1\,. \end{cases} \tag{36}$$

Here, the second equation states that u will play the role of r^{-1}, and the first equation provides the solution r of equation (34), without involving the inversion r^{-1} of the unknown function. Thus, the Galerkin projection can be precomputed, providing a reduced-order model for the couple $(r,\, u)$. It is important to see that this reduced-order model requires not only the proper orthogonal decomposition (35) of the Boltzmann factor r, but also the POD $\widehat{u}_\star = \sum_{e=1}^{n_u} c^e \phi_e^u$ of the scalar field u.

In the sequel, we manage to construct POD-ROM for NPPB using equation (33) or equation (36).

3.2 ROM of the Poisson-Boltzmann equation

3.2.1 Galerkin projection

To get started, let us write the weak form of equation (33)

$$\begin{aligned} \epsilon_v \int_{\mathrm{Y_f}} (\nabla r \cdot \nabla q)\, r \,\mathrm{dY} + 2\epsilon_v \int_{\mathrm{Y_f}} (\nabla r \cdot \nabla r)\, q \,\mathrm{dY} + FBC_\mathrm{b} \left(\int_{\mathrm{Y_f}} r^3\, q \,\mathrm{dY} - \int_{\mathrm{Y_f}} r\, q \,\mathrm{dY} \right) \\ + B\sigma \int_{\mathrm{S_{sf}}} r^2\, q \,\mathrm{dS} = 0, \quad \forall q \in W_{\boldsymbol{\rho}}. \end{aligned} \tag{37}$$

The presence of the cubic term r^3 is an issue. Indeed, the ROM of equation (37), pulled back in the reference domain $\mathrm{Y_f^\star}$, involves:

$$\int_{\mathrm{Y_f^\star}} \phi_i^r\, \phi_j^r\, \phi_k^r\, \phi_l^r\, \widehat{j_{\boldsymbol{\rho}}} \,\mathrm{dY}^\star \tag{38}$$

for all i, j, k, l in $1, \ldots, n_r$, and where $(\phi_i^r)_i$ are the POD modes of the salar function r. For example, when $n_r = 5$, this involves 625 integral computations, including $O(n_\mathrm{dof})$ operations each. Although it is possible to reduce this arithmetical complexity by taking the symmetrical roles of i, j, k and l into account, it is not sufficient to thwart the $O({n_r}^4)$ increase of the number of operations involved by the Galerkin projection. For this reason, we give up this approach for the POD-ROM computation of $\boldsymbol{D}^\mathrm{hom}$, we will focus on the coupled problems (36) instead.

Let us write the problem to reduce on the reference domain $\mathrm{Y_f^\star}$. We have

$$\left\{\begin{array}{ll} \epsilon_v \displaystyle\int_{\mathrm{Y_f^\star}} u_\star \, \boldsymbol{J}_\rho^{-\intercal} \nabla r_\star \cdot \boldsymbol{J}_\rho^{-\intercal} \nabla q_\star \, \widehat{j_{\boldsymbol{\rho}}} \, \mathrm{dY^\star} + C_\mathrm{b} B \displaystyle\int_{\mathrm{Y_f^\star}} r_\star q_\star \, \widehat{j_{\boldsymbol{\rho}}} \mathrm{dY^\star} = C_\mathrm{b} B \displaystyle\int_{\mathrm{Y_f^\star}} u_\star q_\star \, \widehat{j_{\boldsymbol{\rho}}} \mathrm{dY^\star} - B \displaystyle\int_{\mathrm{S_{sf}^\star}} \sigma q_\star \, g_{\boldsymbol{\rho}} \, \mathrm{dS^\star} & \forall q_\star \\ \displaystyle\int_{\mathrm{Y_f^\star}} r_\star \, u_\star \, q_\star \, \widehat{j_{\boldsymbol{\rho}}} \mathrm{dY^\star} = \displaystyle\int_{\mathrm{Y_f^\star}} q_\star \, \widehat{j_{\boldsymbol{\rho}}} \, \mathrm{dY^\star} & \forall q_\star \end{array}\right. \tag{39}$$

where the weak equation $\displaystyle\int_{\mathrm{Y_f}} r_\star \, u_\star \, q_\star \, \widehat{j_{\boldsymbol{\rho}}} \, \mathrm{dY^\star} = \int_{\mathrm{Y_f}} q_\star \, \widehat{j_{\boldsymbol{\rho}}} \, \mathrm{dY^\star}$ is derived from equation $ru = 1$.

Galerkin projection of equation (39) consists in substituting:

$$r_\star = \sum_{i=1}^{n_r} b^i \phi_i^r \; ; \; u_\star = \sum_{e=1}^{n_u} c^e \phi_e^u \tag{40}$$

and taking the generic ϕ_l^r (respectively ϕ_f^u) as test functions in the first (respectively the second) equation. It particularly requires to do a POD on the inverse Boltzmann factor $u_\star$. It results in the following, nonlinear reduced problem

$$\left\{\begin{array}{ll} \epsilon_v \displaystyle\sum_{i=1}^{n_r} \sum_{e=1}^{n_r^*} \boldsymbol{A}^\rho{}_{ile} b^i c^e + F C_\mathrm{b} B \left(\sum_{i=1}^{n_r} \boldsymbol{D}^\rho{}_{il} b^i - \sum_{e=1}^{n_r^*} \boldsymbol{G}^\rho{}_{le} c^e \right) = -B\sigma \boldsymbol{f}^\rho{}_l & \forall l \in 1, \ldots, n_r \\ \displaystyle\sum_{i=1}^{n_r} \sum_{e=1}^{n_r^*} \boldsymbol{C}^\rho{}_{eif} b^i c^e = \boldsymbol{h}^\rho{}_f & \forall f \in 1, \ldots, n_r^* \end{array}\right. \tag{41}$$

with

$$\boldsymbol{f}^\rho{}_l = \int_{\mathrm{S_{sf}^\star}} \phi_l^r \, g_{\boldsymbol{\rho}} \, \mathrm{dS^\star} \tag{42}$$

$$\boldsymbol{A}^\rho{}_{ile} = \int_{\mathrm{Y_f^\star}} \left(\boldsymbol{J}_\rho{}^{-\intercal} \nabla_{\boldsymbol{\xi}} \phi_i^r \right) \cdot \left(\boldsymbol{J}_\rho{}^{-\intercal} \nabla_{\boldsymbol{\xi}} \phi_l^r \right) \phi_e^u \, \widehat{j_{\boldsymbol{\rho}}} \, \mathrm{dY^\star} \tag{43}$$

$$\boldsymbol{D}^\rho{}_{il} = \int_{\mathrm{Y_f^\star}} \phi_l^r \, \phi_l^r \, \widehat{j_{\boldsymbol{\rho}}} \, \mathrm{dY^\star} \tag{44}$$

$$\boldsymbol{G}^\rho{}_{le} = \int_{\mathrm{Y_f^\star}} \phi_l^r \, \phi_e^u \, j_\rho \, \mathrm{dY^\star} \tag{45}$$

$$\boldsymbol{h}^\rho{}_f = \int_{\mathrm{Y_f^\star}} \phi_f^u \, \widehat{j_{\boldsymbol{\rho}}} \, \mathrm{dY^\star} \tag{46}$$

$$\boldsymbol{C}^\rho{}_{eif} = \int_{\mathrm{Y_f^\star}} \phi_e^u \, \phi_i^r \, \phi_f^u \, \widehat{j_{\boldsymbol{\rho}}} \, \mathrm{dY^\star} \tag{47}$$

Provided these coefficients are calculated, the nonlinear algebraic equations (41) are resolved by either using Newton method, or computing alternatively coefficents b^i and c^e in an iterative procedure, which converges according to a fixed-point property. The performances of both methods are very close. The fixed-point method has been retained for the numerical applications presented in this work, since its implementation is simpler.

3.2.2 Explicit ROM coefficients

Computing, for any value of $\boldsymbol{\rho}$, tensor $\boldsymbol{D}^{\mathrm{hom}}(\boldsymbol{\rho})$ in a reduced time using equations (29), (30) and (41), requires that the integral expressions which result from Galerkin projection are precomputed, independently from the geometrical parameter. Scalar or tensor fields $\boldsymbol{\xi} \mapsto \widehat{j_{\boldsymbol{\rho}}}$, $\boldsymbol{\xi} \mapsto \widehat{\boldsymbol{J}_{\boldsymbol{\rho}}}^{-1}$ and $\boldsymbol{\xi} \mapsto g_{\boldsymbol{\rho}}$ must then be decomposed into expressions where space variable $\boldsymbol{\xi}$ and geometrical parameter $\boldsymbol{\rho}$ are separated. In [28], the authors derive such decompositions from the explicit formulas (B.77)–(B.78), when the EDL effects are neglected. This method is recalled in the appendix B.3, and is apparented to Reduced Basis techniques that and have been widely

used in the context of fluid mechanics [17, 24, 34] [4].The full and reduced problem set on the reference domain are thus said to be affinely dependent from the parameter $\boldsymbol{\rho}$. Formulae (B.90) and (B.98) provide the affine decompositions for $\widehat{j_{\boldsymbol{\rho}}}$ and $g_{\boldsymbol{\rho}}$. Moreover, relation (B.81) proves that $\widehat{\boldsymbol{J}_{\boldsymbol{\rho}}}$ is, for each $\boldsymbol{\xi}$, a symmetrical operator. Thus we have the following expressions

$$\int_{\mathrm{Y_f^\star}} \left(\boldsymbol{J}_\rho{}^{-\intercal}\,\nabla_{\boldsymbol{\xi}}\phi_i^r\right)\cdot\left(\boldsymbol{J}_\rho{}^{-\intercal}\,\nabla_{\boldsymbol{\xi}}\phi_l^r\right)\,\phi_e^u\,\widehat{j_{\boldsymbol{\rho}}}\,\mathrm{dY}^\star = \int_{\mathrm{Y_f^\star}} \left(\boldsymbol{J}_\rho{}^{-2\intercal}\,\widehat{j_{\boldsymbol{\rho}}}\,\nabla_{\boldsymbol{\xi}}\phi_i^r\right)\cdot\nabla_{\boldsymbol{\xi}}\phi_l^r\;\phi_e^u\,\mathrm{dY}^\star \tag{48}$$

where $\boldsymbol{A}^{-\intercal}$ denotes the inverse of the conjugate of matrix $\boldsymbol{A}$. Consequently, to separate $\boldsymbol{\rho}$ and $\boldsymbol{\xi}$ in all integral expressions resulting from Galerkin projection, it is sufficient to achieve this operation for the tensor fields

$$\boldsymbol{\xi}\mapsto\widehat{\boldsymbol{J}_{\boldsymbol{\rho}}}^{-2}\,\widehat{j_{\boldsymbol{\rho}}}. \tag{49}$$

since tensor $\widehat{\boldsymbol{J}_{\boldsymbol{\rho}}}$ and its inverse are symmetric. We notice that variable separation is not directely possible for $\widehat{\boldsymbol{J}_{\boldsymbol{\rho}}}^{-1}$ because of the $\beta_{\rho_n}\|\boldsymbol{\xi}-\boldsymbol{\xi}_n\|+\alpha_{\rho_n}$ denominators. Anyway, these denominators are simplified in expressions (49) thanks to the $\left(\beta_{\rho_n}\|\boldsymbol{\xi}-\boldsymbol{\xi}_n\|+\alpha_{\rho_n}\right)^{d-1}$ factor which appear in (B.90) (see appendix B.3). An affine decomposition will be possible if $d-1-2\geq 2$ (worst case). Nevertheless, this simplicifation depends on the dimension d of the elementary cell Y, which can be 2 or 3. The authors of [28] stated that consequently, an affine decomposition exists exactely if $d=3$, but not if $d=2$. For $d=2$ the decomposition can be approximated by using a truncated power series. Formulae allowing this decomposition are developed in [28] and recalled in appendix B.3. We deduce, from expressions (B.90)–(B.94), coefficients $\boldsymbol{A}^{\boldsymbol{\rho}}{}_{ile}$, $\boldsymbol{C}^{\boldsymbol{\rho}}{}_{eif}$, $\boldsymbol{D}^{\rho}{}_{il}$, $\boldsymbol{G}^{\boldsymbol{\rho}}{}_{le}$, $\boldsymbol{f}^{\boldsymbol{\rho}}{}_{l}$ and $\boldsymbol{h}^{\boldsymbol{\rho}}{}_{f}$ of the ROM (39) of the Boltzmann factor

$$\boldsymbol{C}^{\boldsymbol{\rho}} = \overline{\boldsymbol{C}} + \sum_{n=1}^{n_\mathrm{s}}\sum_{p=0}^{d-1} C_{d-1}^p\,\alpha_{\rho_n}^p\,\beta_{\rho_n}^{d-p}\,\widetilde{\boldsymbol{C}}_{p,n} \tag{50}$$

where $C_{d-1}^p = \dfrac{n!}{(n-p)!p!}$ is the generic binomial coefficient, n_s the number of solid inclusions and with

$$\left[\overline{\boldsymbol{C}}\right]_{eif} = \int_{\mathrm{Y_e^\star}} \phi_e^u\,\phi_i^r\,\phi_f^u\,\mathrm{dY}^\star \quad\text{and}\quad \left[\widetilde{\boldsymbol{C}}_{p,n}\right]_{eif} = \int_{\mathrm{Y_{c,n}^\star}} \phi_e^u\,\phi_i^r\,\phi_f^u\,\frac{1}{\|\,\boldsymbol{\xi}-\boldsymbol{\xi}_n\,\|^p}\,\mathrm{dY}^\star \tag{51}$$

$\boldsymbol{D}^{\boldsymbol{\rho}}$ is written as

$$\boldsymbol{D}^{\boldsymbol{\rho}} = \overline{\boldsymbol{D}} + \sum_{n=1}^{n_\mathrm{s}}\sum_{p=0}^{d-1} C_{d-1}^p\,\alpha_{\rho_n}^p\,\beta_{\rho_n}^{d-p}\,\widetilde{\boldsymbol{D}}_{p,n}, \tag{52}$$

with

$$\left[\overline{\boldsymbol{D}}\right]_{il} = \int_{\mathrm{Y_e^\star}} \phi_l^r\,\phi_l^u\,\mathrm{dY}^\star \quad\text{and}\quad \left[\widetilde{\boldsymbol{D}}_{p,n}\right]_{il} = \int_{\mathrm{Y_{c,n}^\star}} \phi_l^r\,\phi_l^r\,\frac{1}{\|\,\boldsymbol{\xi}-\boldsymbol{\xi}_n\,\|^p}\,\mathrm{dY}^\star. \tag{53}$$

The tensor $\boldsymbol{G}^{\boldsymbol{\rho}}$ is given by

$$\boldsymbol{G}^{\boldsymbol{\rho}} = \overline{\boldsymbol{G}} + \sum_{n=1}^{n_\mathrm{s}}\sum_{p=0}^{d-1} C_{d-1}^p\,\alpha_{\rho_n}^p\,\beta_{\rho_n}^{d-p}\,\widetilde{\boldsymbol{G}}_{p,n}, \tag{54}$$

with

$$\left[\overline{\boldsymbol{G}}\right]_{le} = \int_{\mathrm{Y_e^\star}} \phi_l^r\,\phi_e^u\,\mathrm{dY}^\star \quad\text{and}\quad \left[\widetilde{\boldsymbol{G}}_{p,n}\right]_{le} = \int_{\mathrm{Y_{c,n}^\star}} \phi_l^r\,\phi_e^u\,\frac{1}{\|\,\boldsymbol{\xi}-\boldsymbol{\xi}_n\,\|^p}\,\mathrm{dY}^\star. \tag{55}$$

The other coefficients are given by

[4] See the pedagogical treatise [33] for more information on Reduced Basis Methods.

$$\boldsymbol{f}^{\boldsymbol{\rho}} = \sum_{n=1}^{n_\mathrm{s}} g_{\rho,n}\, \overline{\boldsymbol{f}}_n \quad \text{with} \quad \left[\overline{\boldsymbol{f}}_n\right]_i = \int_{\Gamma_n^\star} \phi_l^r \,\mathrm{dS}^\star. \tag{56}$$

and

$$\boldsymbol{h}^{\rho} = \overline{\boldsymbol{h}} + \sum_{n=1}^{n_\mathrm{s}} \sum_{p=0}^{d-1} C_{d-1}^p \alpha_{\rho_n}^p \beta_{\rho_n}^{d-p} \widetilde{\boldsymbol{h}}_{p,n} \ , \tag{57}$$

with

$$\left[\overline{\boldsymbol{h}}\right]_f = \int_{\mathrm{Y_e^\star}} \phi_f^u \,\mathrm{dY}^\star \quad \text{and} \quad \left[\widetilde{\boldsymbol{h}}_{p,n}\right]_f = \int_{\mathrm{Y_{c,n}^\star}} \phi_f^u \,\frac{1}{\parallel \boldsymbol{\xi} - \boldsymbol{\xi}_n \parallel^p} \,\mathrm{dY}^\star \ . \tag{58}$$

Finally, the tensor $\boldsymbol{A}^{\boldsymbol{\rho}}$ is expressed approximately as

$$\begin{aligned} \boldsymbol{A}^{\boldsymbol{\rho}} \simeq \overline{\boldsymbol{A}} + \sum_{n=1}^{n_\mathrm{s}} \left(\widetilde{\boldsymbol{A}}_{0,0,n} + \frac{\alpha_{\rho_n}}{\beta_{\rho_n}} \widetilde{\boldsymbol{A}}_{1,0,n} \right) - \sum_{n=1}^{n_\mathrm{s}} \left(1 + \beta_{\rho_n}^{N_\mathrm{dev}+1} \right) \frac{\alpha_{\rho_n}}{\beta_{\rho_n}} \widetilde{\boldsymbol{A}}_{0,1,n} \\ + \sum_{n=1}^{n_\mathrm{s}} \sum_{p=1}^{N_\mathrm{dev}} (-1)^p \left(\sum_{m=p}^{N_\mathrm{dev}} \beta_{\rho_n}^m C_m^p \right) (1-\beta_{\rho_n}) \frac{\alpha_{\rho_n}}{\beta_{\rho_n} q^p} \widetilde{\boldsymbol{A}}_{p,1,n} \ , \end{aligned} \tag{59}$$

with

$$\left[\overline{\boldsymbol{A}}\right]_{ile} = \int_{\mathrm{Y_e^\star}} \phi_e^u \nabla_{\boldsymbol{\xi}} \phi_i^r \cdot \nabla_{\boldsymbol{\xi}} \phi_l^r \,\mathrm{dY}^\star, \tag{60}$$

$$\left[\widetilde{\boldsymbol{A}}_{p,0,n}\right]_{ile} = \int_{\mathrm{Y_{c,n}^\star}} \phi_e^u \frac{\nabla_{\boldsymbol{\xi}} \phi_i^r \cdot \nabla_{\boldsymbol{\xi}} \phi_l^r}{\parallel \boldsymbol{\xi} - \boldsymbol{\xi}_n \parallel^p} \,\mathrm{dY}^\star \ , \tag{61}$$

$$\left[\widetilde{\boldsymbol{A}}_{p,1,n}\right]_{ile} = \int_{\mathrm{Y_{c,n}^\star}} \phi_e^u \left(\|\boldsymbol{\xi} - \boldsymbol{\xi}_n\|^{p-1} \boldsymbol{G}_{\boldsymbol{u}(\boldsymbol{\xi}-\boldsymbol{\xi}_n)} \nabla_{\boldsymbol{\xi}} \phi_i^r \right) \cdot \nabla_{\boldsymbol{\xi}} \phi_l^r \,\mathrm{dY}^\star \ . \tag{62}$$

where N_dev is the number of terms that are kept, in the case of $d = 2$, in the power series of $\widehat{\boldsymbol{J}_{\boldsymbol{\rho}}}^{-2} \widehat{j_{\boldsymbol{\rho}}}$. It must be noticed that these coefficients are independent from $\boldsymbol{\rho}$ and are precomputed once and for all.

3.3 ROM for the NPPB problem

Like in subsection 3.2.2, the symmetry of operator $\widehat{\boldsymbol{J}_{\boldsymbol{\rho}}}$ for all $\boldsymbol{\xi}$ can be employed to reformulate the integral expressions over fluid domains, which appear in (29)–(30), as:

$$\int_{\mathrm{Y_f^\star}} \phi_i^r \,\nabla\, \boldsymbol{\phi}_j \,\widehat{\boldsymbol{J}_{\boldsymbol{\rho}}}^{-1} : \nabla \boldsymbol{\phi}_l \,\widehat{\boldsymbol{J}_{\boldsymbol{\rho}}}^{-1} \,\widehat{j_{\boldsymbol{\rho}}} \,\mathrm{dY}^\star = \int_{\mathrm{Y_f^\star}} \phi_i^r \,\nabla\, \boldsymbol{\phi}_j \,\widehat{\boldsymbol{J}_{\boldsymbol{\rho}}}^{-2} \,\widehat{j_{\boldsymbol{\rho}}} : \nabla \boldsymbol{\phi}_l \,\mathrm{dY}^\star \tag{63}$$

$$\int_{\mathrm{Y_f^\star}} \widehat{\boldsymbol{J}_{\boldsymbol{\rho}}}^{-\intercal} \nabla \phi_i^r \cdot \boldsymbol{\phi}_l \,\widehat{j_{\boldsymbol{\rho}}} \,\mathrm{dY}^\star = \int_{\mathrm{Y_f^\star}} \left(\widehat{\boldsymbol{J}_{\boldsymbol{\rho}}}^{-1} \,\widehat{j_{\boldsymbol{\rho}}} \right)^\intercal \nabla \phi_i^r \cdot \boldsymbol{\phi}_l \,\mathrm{dY}^\star \tag{64}$$

$$\int_{\mathrm{Y_f^\star}} \phi_i^r \left(\nabla_{\boldsymbol{\xi}} \,\boldsymbol{\phi}_l \,\widehat{\boldsymbol{J}_{\boldsymbol{\rho}}}^{-1} \right)^\intercal \widehat{j_{\boldsymbol{\rho}}} \,\mathrm{dY}^\star = \int_{\mathrm{Y_f^\star}} \phi_i^r \left(\nabla_{\boldsymbol{\xi}} \,\boldsymbol{\phi}_l \,\widehat{\boldsymbol{J}_{\boldsymbol{\rho}}}^{-1} \,\widehat{j_{\boldsymbol{\rho}}} \right)^\intercal \mathrm{dY}^\star \,. \tag{65}$$

$$\tag{66}$$

These expressions are involved in the computation of $\widehat{\boldsymbol{\chi}}_\star$ and $\widehat{\boldsymbol{D}}^\mathrm{hom}$. Consequently, variables $\boldsymbol{\rho}$ and $\boldsymbol{\xi}$ can be separated in all integral expressions resulting from Galerkin projection, if this operation is done for tensor fields:

$$\boldsymbol{\xi} \mapsto \widehat{\boldsymbol{J}_{\boldsymbol{\rho}}}^{-1} \,\widehat{j_{\boldsymbol{\rho}}} \quad \text{and} \quad \boldsymbol{\xi} \mapsto \widehat{\boldsymbol{J}_{\boldsymbol{\rho}}}^{-2} \,\widehat{j_{\boldsymbol{\rho}}}. \tag{67}$$

Formulae providing $\widehat{\boldsymbol{\chi}}_\star$ and $\widehat{\boldsymbol{D}}^\mathrm{hom}$ are similar, they are sent into Appendix C for the sake of clarity.

3.4 Summary of the method

The reduced-order model developed in this section for periodic homogenization consists in the following steps:

Offline 1. Using firstly equation (39) and secondly equation (28), compute the snpshots[5] $r_\star(\boldsymbol{\xi},\rho_1)$, … , $r_\star(\boldsymbol{\xi},\boldsymbol{\rho}_{n_{\text{snap}}})$, $u_\star(\boldsymbol{\xi},\rho_1)$, … , $u_\star(\boldsymbol{\xi},\boldsymbol{\rho}_{n_{\text{snap}}})$ and $\boldsymbol{\chi}_\star(\boldsymbol{\xi},\boldsymbol{\rho}_1)$, … , $\boldsymbol{\chi}_\star(\boldsymbol{\xi},\boldsymbol{\rho}_{n_{\text{snap}}})$, for a sample $\{\boldsymbol{\rho}_1,\dots,\boldsymbol{\rho}_{n_{\text{snap}}}\}$ of parameter values where $r_\star = e^{-B\varphi_\star}$ and $u_\star = e^{+B\varphi_\star}$;

2. Compute correlation tensors $[\boldsymbol{C}^{\boldsymbol{\chi}}]_{jk} = \displaystyle\int_{\mathrm{Y}_{\mathrm{f}}^\star} \boldsymbol{\chi}_\star(\boldsymbol{\xi};\boldsymbol{\rho}_j)\cdot\boldsymbol{\chi}_\star(\boldsymbol{\xi};\boldsymbol{\rho}_k)\,\mathrm{dY}^\star$, $[\boldsymbol{C}^{r}]_{il} = \displaystyle\int_{\mathrm{Y}_{\mathrm{f}}^\star} r_\star(\boldsymbol{\xi};\boldsymbol{\rho}_i)\,r_\star(\boldsymbol{\xi};\boldsymbol{\rho}_l)\,\mathrm{dY}^\star$
$[\boldsymbol{C}^{u}]_{ef} = \displaystyle\int_{\mathrm{Y}_{\mathrm{f}}^\star} u_\star(\boldsymbol{\xi};\boldsymbol{\rho}_e)\,u_\star(\boldsymbol{\xi};\boldsymbol{\rho}_f)\,\mathrm{dY}^\star$;

3. Build basis $(\boldsymbol{\phi}_j)_{j=1}^{n_{\text{snap}}}$, $(\phi_i^r)_i^{n_{\text{snap}}}$ and $(\phi_e^u)_e^{n_{\text{snap}}}$;

4. Determine the truncation indexes $n_{\boldsymbol{\chi}}$, n_r and n_u such that

$$\boldsymbol{\chi}_\star(\boldsymbol{\rho},\boldsymbol{\xi}) \simeq \sum_{j=1}^{n_{\boldsymbol{\chi}}} a_j(\boldsymbol{\rho})\boldsymbol{\phi}_j(\boldsymbol{\xi}) \quad ; \quad r_\star(\boldsymbol{\rho},\boldsymbol{\xi}) \simeq \sum_{i=1}^{n_r} b_i(\boldsymbol{\rho})\phi_i^r(\boldsymbol{\xi}) \quad ; \quad u_\star(\boldsymbol{\rho},\boldsymbol{\xi}) \simeq \sum_{e=1}^{n_u} a_e(\boldsymbol{\rho})\phi_e^u(\boldsymbol{\xi})\,,$$

according to the criterion seen in the appendix A (Equation (A.74)).

5. Using the POD modes obtained in step 4, compute coefficients $\big[\overline{\boldsymbol{A}}\big]_{ile}$, $\big[\widetilde{\boldsymbol{A}}_{0,0,n}\big]_{ile}$, $\big[\widetilde{\boldsymbol{A}}_{0,1,n}\big]_{ile}$, $\big[\overline{\boldsymbol{C}}\big]_{eif}$, $\big[\widetilde{\boldsymbol{C}}\big]_{eif}$, $\big[\widetilde{\boldsymbol{D}}\big]_{il}$, $\big[\overline{\boldsymbol{D}}\big]_{il}$, $\big[\overline{\boldsymbol{G}}\big]_{le}$, $\big[\widetilde{\boldsymbol{G}}\big]_{le}$, $\big[\overline{\boldsymbol{f}}\big]_{l}$, $\big[\overline{\boldsymbol{f}}\big]_{l}$, $\big[\overline{\boldsymbol{h}}\big]_{f}$, $\big[\widetilde{\boldsymbol{h}}\big]_{f}$ (formulae (50)–(62)) ;
and coefficients $\big[\overline{\boldsymbol{C}^{\boldsymbol{\chi}}}\big]_{ki}$, $\big[\widetilde{\boldsymbol{C}^{\boldsymbol{\chi}}}_n\big]_{ki}$, $\overline{\boldsymbol{s}}$, $\big[\widetilde{\boldsymbol{s}}_p\big]_i$, $\big[\overline{\boldsymbol{A}^{\boldsymbol{\chi}}}\big]_{jki}$, $\big[\widetilde{\overline{\boldsymbol{A}^{\boldsymbol{\chi}}}}_{p,0}\big]_{jki}$, $\big[\widetilde{\overline{\boldsymbol{A}^{\boldsymbol{\chi}}}}_{p,1}\big]_{jki}$, $\big[\widetilde{\overline{\boldsymbol{A}^{\boldsymbol{\chi}}}}_{p,1}\big]_{jki}$, $\big[\overline{\boldsymbol{B}^{\boldsymbol{\chi}}}\big]_{ki}$, $\big[\widetilde{\overline{\boldsymbol{B}^{\boldsymbol{\chi}}}}_{p,0}\big]_{ki}$, $\big[\widetilde{\overline{\boldsymbol{B}^{\boldsymbol{\chi}}}}_{p,1}\big]_{ki}$, $\big[\overline{\boldsymbol{K}^{r}}_{ji}\big]_{ab}$, $\big[\widetilde{\overline{\boldsymbol{K}^{r}}}_{(p,0)\ ji}\big]_{ab}$, $\big[\widetilde{\overline{\boldsymbol{K}^{r}}}_{(p,1)\ ji}\big]_{ab}$, (appendix C).

Online For $\boldsymbol{\rho} \notin \{\boldsymbol{\rho}_1,\dots,\boldsymbol{\rho}_{n_{\text{snap}}}\}$:

1. Update $\boldsymbol{A}^{\rho}{}_{ile}$, $\boldsymbol{D}^{\rho}{}_{il}$, $\boldsymbol{G}^{\rho}{}_{le}$, $\boldsymbol{h}^{\rho}{}_{f}$, $\boldsymbol{C}^{\rho}{}_{eif}$, $\boldsymbol{f}^{\rho}{}_{l}$, from coefficients $\big[\overline{\boldsymbol{A}}\big]_{ile}$, $\big[\widetilde{\boldsymbol{A}}_{0,0,n}\big]_{ile}$, $\big[\widetilde{\boldsymbol{A}}_{0,1,n}\big]_{ile}$, $\big[\overline{\boldsymbol{C}}\big]_{eif}$, $\big[\widetilde{\boldsymbol{C}}\big]_{eif}$, $\big[\widetilde{\boldsymbol{D}}\big]_{il}$, $\big[\overline{\boldsymbol{D}}\big]_{il}$, $\big[\overline{\boldsymbol{G}}\big]_{le}$, $\big[\widetilde{\boldsymbol{G}}\big]_{le}$, $\big[\overline{\boldsymbol{f}}\big]_{l}$, $\big[\overline{\boldsymbol{f}}\big]_{l}$, $\big[\overline{\boldsymbol{h}}\big]_{f}$, $\big[\widetilde{\boldsymbol{h}}\big]_{f}$ (see formulae (59), (50), (52), (54), (56), (59)) ;
update coefficients $\boldsymbol{A}^{\boldsymbol{\chi}}_{\boldsymbol{\rho}\,jli}$, $\boldsymbol{B}^{\boldsymbol{\chi}}_{\boldsymbol{\rho}\,li}$, $\boldsymbol{C}^{\boldsymbol{\chi}}_{\boldsymbol{\rho}\,li}$, $\boldsymbol{s}_{\boldsymbol{\rho}\,i}$, $\Big[\boldsymbol{K}^{r}_{\boldsymbol{\rho}\,ij}\Big]_{ab}$, (see appendix C).
2. Resolution of the nested ROMs (41) and (29) to obtain $(b_i)_i(\boldsymbol{\rho})$ and $(a_j)_j(\boldsymbol{\rho})$
3. Computation in a reduced time of tensor $\widehat{\boldsymbol{D}}^{\text{hom}}(\boldsymbol{\rho})$ estimated by ROM from relation (30).

The Offline part, which involves the costly Snapshot computation with Finite Element Method, the correlation tensor structure and the Galerkin projection, is done only one time. Online ROM computations can then be done, in a reduced time, for a great number of values of ρ.

4 Numerical results

In this section, we illustrate the accuracy and the reduced computational cost of the proposed method. We primarily focus on the ability of the method to approximate the homogenized diffusion tensor $\boldsymbol{D}^{\text{hom}}$ given by equation (11) when D is constant. However, the latter may be split in two terms as follows:

$$\boldsymbol{D}^{\text{hom}} = s^{\text{hom}}\boldsymbol{I} + \boldsymbol{T}^{\text{hom}}, \qquad s^{\text{hom}} = \frac{D}{|\Omega|}\int_{\mathrm{Y_f}} e^{-B\varphi}\mathrm{dY} \text{ and } \boldsymbol{T}^{\text{hom}} = \frac{D}{|\Omega|}\int_{\mathrm{Y_f}} e^{-B\varphi}\nabla_{\boldsymbol{y}}\boldsymbol{\chi}^{\intercal}\mathrm{dY}\,. \tag{68}$$

As the computation of the the first part is easy for all geometries, focus will be done on the computation of $\boldsymbol{T}^{\text{hom}}$ which is more challenging. In the next, the results obtained by solving the full-order model FOM and the reduced-order are compared. FOM corresponds to the classical full-order finite-element model associated with (32) defined over the physical domain which is remeshed for every value of the geometry parameter, ROM denotes the reduced order model constructed from snapshots $\boldsymbol{\chi}_\star(\boldsymbol{\xi};\boldsymbol{\rho}_j)$, $r_\star(\boldsymbol{\xi};\boldsymbol{\rho}_i)$, $u_\star(\boldsymbol{\xi};\boldsymbol{\rho}_e)$, themselves computed using full-order equations (28)–(39) set on $\mathrm{Y}_{\mathrm{f}}^\star$.

The accuracy will be studied by considering the relative error between the FOM and the ROM solutions, defined as:

[5] In this work, for the numerical applications, the snapshots for $r_\star$ and $u_\star$ were obtained from relations $r_\star = e^{-B\varphi_\star}$ and $u_\star = e^{+B\varphi_\star}$, where $\varphi_\star$ came from the full-order Poisson-Boltzmann equation (12) pulled-back on $\mathrm{Y}_{\mathrm{f}}^\star$.

$$e_v = \frac{v^{\mathrm{ROM}} - v^{\mathrm{FOM}}}{v^{\mathrm{FOM}}} \tag{69}$$

where $v = s^{\mathrm{hom}}$, T_{ij}^{hom} or D_{ij}^{hom} is a scalar $\boldsymbol{\rho}$-dependent homogenized coefficient. On the other hand, for the scalar-valued (respectively vector-valued) function $v = r$ (respectively $\boldsymbol{v} = \boldsymbol{\chi}$), the following error

$$e_{\boldsymbol{v}} = \frac{\|\widehat{\boldsymbol{v}}_{\mathrm{ref}} \circ \widehat{\boldsymbol{\tau}_{\boldsymbol{\rho}}}^{-1} - \boldsymbol{v}\|_{V_\rho}}{\|\boldsymbol{v}\|_{V_\rho}} \tag{70}$$

between the ROM and full-order solutions will be evaluated on the physical domain $\mathrm{Y_f}$. All programs have been written in Python3 using packages from the FEniCS project, and executed on 4 CPU cadenced at 2.90GHz, with 16GB of working memory. In all this section, the full order solutions FOM are computed with quadratic Lagrange elements.

4.1 Single spherical inclusion

The first microstructure for which POD-ROM is performed to compute tensor $\boldsymbol{D}^{\mathrm{hom}}$ and $\boldsymbol{T}^{\mathrm{hom}}$ consists in the periodic repetition of a cubical cell with a single spherical solid inclusion located at the center of the cell (see figure 3). According to the symmetry of the elementary cell, the tensor $\boldsymbol{D}^{\mathrm{hom}}$ exhibits isotropic properties. Therefore, we limit the presentation of results to the tensor components D_{11}^{hom} and T_{11}^{hom}.

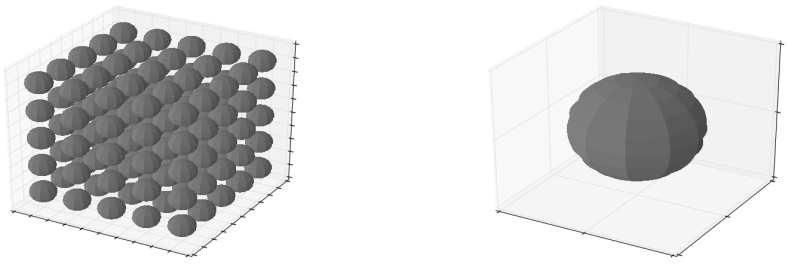

(a) Periodical microstructure (b) Elementary cell

Fig. 3: Three dimensional periodical microstructure and associated REV fluid domain with single solid spherical inclusion parametrized by its radius ρ.

4.1.1 POD-ROM construction

The POD bases are built by considering 6 snapshots corresponding to values $\{0.45, 0.55, \ldots, 0.95\}$ of radius ρ. For this range of radius, the volume fraction of the fluid phase varies between 0.29 and 0.87. The POD bases for ROM are truncated to 4 and 5 modes respectively, using the so-called energy criterion with $\nu = 10^{-4}$ of POD (99, 99% of representativity, see appendix A). The transformation $\boldsymbol{\tau}_\rho$ is built with the reference radius $\rho_{\mathrm{ref}} = 0.8$. The POD-ROM is tested for the 10 values $\{0.475, 0.525, \ldots, 0.925\}$ of $\tilde{\rho}$, which do not belong to the training set. Physical paramters are $F = 96490\,\mathrm{C \cdot mol^{-1}}$, $R = 8.3143\,\mathrm{J.K.mol^{-1}}$, $\epsilon_v = 80 \cdot 8.854 \cdot 10^{-12}\,\mathrm{F.m^{-1}}$ and $T = 293\,\mathrm{K}$. The ROM is tested for 4 sets of the pair (C_{b}, σ):

- $C_{\mathrm{b}} = 500\,\mathrm{mol.m^{-3}}$ and $\sigma = -0.02\,\mathrm{C.m^{-2}}$,
- $C_{\mathrm{b}} = 500\,\mathrm{mol.m^{-3}}$ and $\sigma = -0.2\,\mathrm{C.m^{-2}}$,
- $C_{\mathrm{b}} = 100\,\mathrm{mol.m^{-3}}$ and $\sigma = -0.01\,\mathrm{C.m^{-2}}$,
- $C_{\mathrm{b}} = 20\,\mathrm{mol.m^{-3}}$ and $\sigma = -0.01\,\mathrm{C.m^{-2}}$.

4.1.2 Homogenized coefficients

Firstly, the results obtained on s^{hom} are evaluated, these are summarized on figure 4.

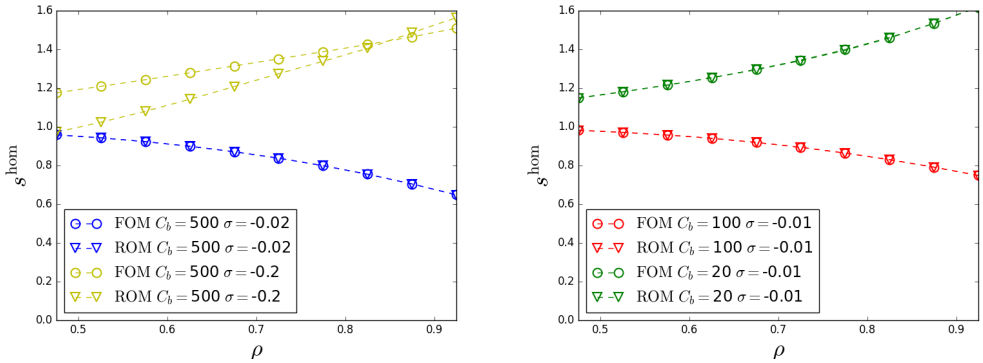

(a) Two values of σ (b) Two values of C_{b}

Fig. 4: Comparison of the coefficients s^{hom} obtained by the FOM and by the ROM for 4 values of (C_{b}, σ)

Figure 4 shows the s^{hom} values obtained with FOM method (respectively ROM method), plotted by circles (respectively triangles). More precisely, the values of s^{hom} obtained by ROM are defined by $\widehat{s^{\text{hom}}} = \frac{1}{|\mathrm{Y}^\star|} \sum_{i=1}^{n_r} b^i \, \boldsymbol{s}_{\boldsymbol{\rho}_i}$, according to equation (30). The obtained value are sensitively the same, except from $\sigma = -0.2\,\mathrm{C.m}^{-2}$ when $\rho < 0.7$. The latter case is characterized by a relatively high value of the surface charge due to the adsorbed ions, and then a relatively important influence of EDL. However, this is combined with a large porosity, which isn't realistic for cementitious media.

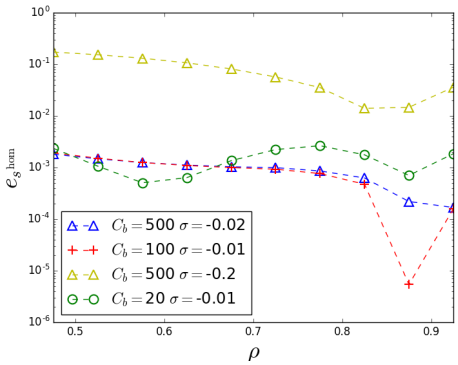

Fig. 5: Relative errors between the values of s^{hom} obtained by the ROM and those obtained by the FOM for 4 values of (C_{b}, σ)

Figure 5 presents the ROM error of $\widehat{s^{\text{hom}}}$ estimator. This error is computed with formula (69). We see that the ROM error comparatively to FOM is less than 1% except if $\sigma = -0.2\,\mathrm{C.m}^{-2}$. In the latter case, $\widehat{s^{\text{hom}}}$ errors are less than 9%, and even 2% if $\rho \in [0.7, 0.93]$. This is of huge relevance since the error on $\widehat{s^{\text{hom}}}$ measures the accuracy of the ROM of the Boltzmann factor.

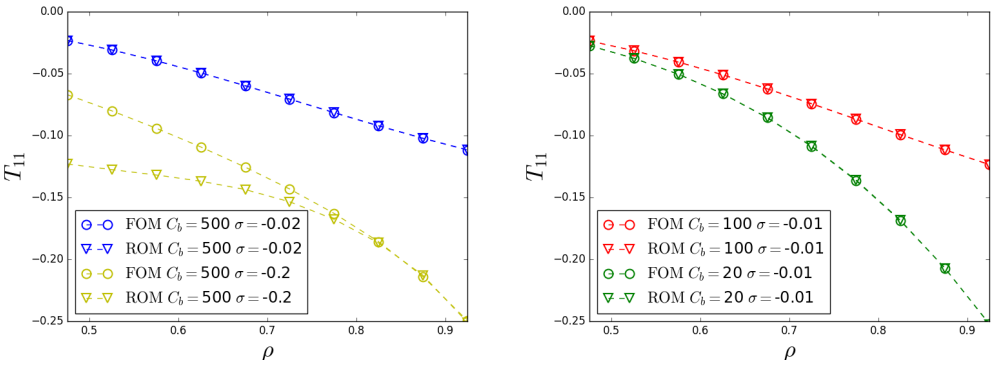

(a) Two values of σ (b) Two values of C_b

Fig. 6: Comparison of the coefficients T_{11}^{hom} obtained by the FOM and by the ROM for 4 values of (C_b, σ)

With the conventions of figure 4, figure 6 shows the values of the first coefficient T_{11}^{hom} of the tortuosity tensor $\boldsymbol{T}^{\mathrm{hom}}$. The default values, obtained with FEM, are compared to the first coefficient of $\widehat{\boldsymbol{T}^{\mathrm{hom}}} = \dfrac{1}{|\mathrm{Y}^\star|} \sum\limits_{i=1}^{n_r} b^i \sum_{j=1}^{n_\chi} a^j \boldsymbol{K}^r_{\boldsymbol{\rho}ij}$, see again (30). According to figure 6, the ROM is able to correctly predict the value of T_{11}^{hom} except from the small values of ρ in the case where $\sigma = -0.2\,\mathrm{C.m^{-2}}$.

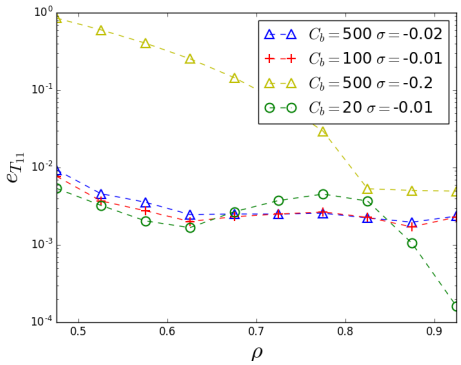

Fig. 7: Relative errors between the values of T_{11}^{hom} obtained by the ROM and those obtained by the FOM for 4 values of (C_b, σ)

Figure 7 presents the ROM error on coefficient T_{11}^{hom}, computed with formula (69). It confirms the observations made with figure 6. In particular, ROM errors are less than 1% unless $\sigma = -0.2\,\mathrm{C.m^{-3}}$. For fixed values of physical parameters C_b et σ, errors are more important for low values of ρ (large porosity), they eventually reach 7% when $C_\mathrm{b} = 20\,\mathrm{mol.m^{-3}}$. For $\sigma = -0.2\,\mathrm{C.m^{-3}}$, ROM errors are more important. These are however less than 4% if $\rho \geq 0.7$.

We recall that D_{11}^{hom} values are the sum of s^{hom} and T_{11}^{hom}. Thus, and according to figures 4 and 6, ROM estimations of D_{11}^{hom} are sensibly the same than values obtained with the full model FOM when $\sigma \neq -0.2\,\mathrm{C.m^{-3}}$, or when $\sigma = -0.2\,\mathrm{C.m^{-3}}$ and $\rho \geq 0.7$.

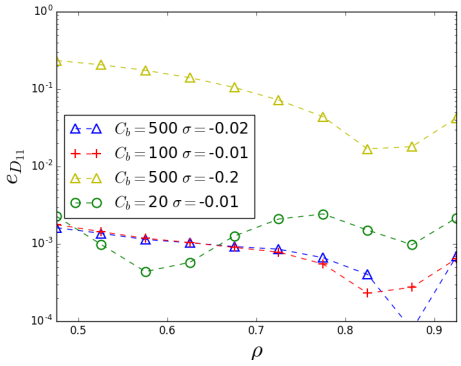

Fig. 8: Relative errors between the values of D_{11}^{hom} obtained by the ROM and those obtained by the FOM for 4 values of (C_{b}, σ)

We see more precisely on figure 8 that D_{11}^{hom} estimation errors are less than 1% if $\sigma \neq -0.2\,\text{C.m}^{-2}$. When $\sigma = -0.2\,\text{C.m}^{-2}$ and $\rho \geq 0.7$, the estimation error of D_{11}^{hom} is less than 10%.

4.1.3 Scalar and vector fields

Finally, figure 9 (respectively 9a) presents the ROM errors on the Boltzmann factor r (respecively $\boldsymbol{\chi}$), computed using formula (70).

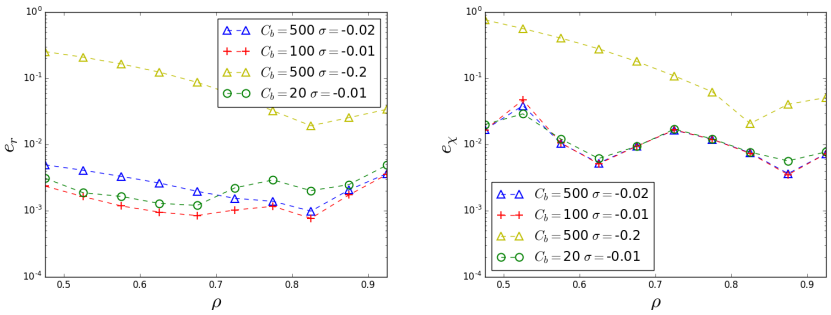

(a) $e\ r$ (b) $e\ \boldsymbol{\chi}$

Fig. 9: Relative errors between the fields r and $\boldsymbol{\chi}$ obtained by the ROM and those obtained by the FOM for 4 values of (C_{b}, σ)

According to figure 9a, the error made by the estimator $\widehat{r}_\star$ is less than 1%, when $\sigma \neq -0.2\,\text{C.m}^{-2}$. If $\sigma = -0.2\,\text{C.m}^{-2}$, the ROM error stays below 9%, moreover it is less than 4% if $= \rho \geq 0.625$. This error is associated with important differences between ρ and $\rho_\star$, which happen when porosity is large. According to figure 9b, ROM errors on $\boldsymbol{\chi}$ are less than 4% for all ρ, if $\sigma \neq -0.2\,\text{C.m}^{-3}$. When $\sigma = -0.2\,\text{C.m}^{-3}$, ROM errors are less than 10% if $\rho \geq 0.7$, e.g if the porosity is low.

4.1.4 Computing performances

Figure 10 presents, for all tested parameter values $\tilde{\rho}$, the time of execution of the FOM model (respectivement the ROM model), which compute $\boldsymbol{D}^{\text{hom}}$ (respectively its estimation $\widehat{\boldsymbol{D}}^{\text{hom}}$). This time of execution includes $\widehat{r}_\star$ computation, $\widehat{s^{\text{hom}}}$ construction, $\widehat{\boldsymbol{\chi}}_\star$ and $\widehat{\boldsymbol{T}^{\text{hom}}}$ estimation.

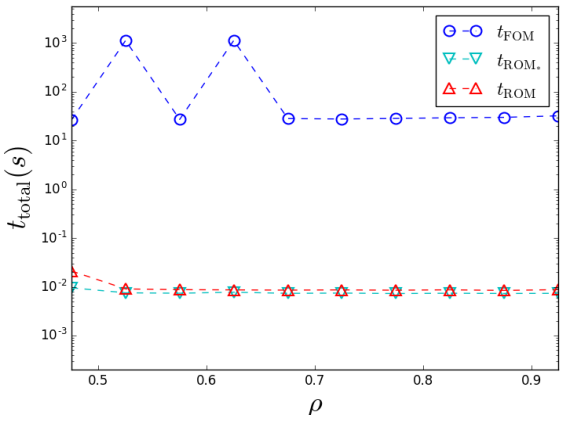

Fig. 10: Time elapsed to compute $\widehat{\boldsymbol{D}}^{\text{hom}}$ for $\sigma = -0.01\,\text{C.m}^2$ and $C_\text{b} = 100\,\text{mol.m}^{-3}$

Figure 10 presents the time of execution of the ROM. In the worst case, the computation of $\boldsymbol{D}^{\text{hom}}$ is 3 000 times faster than using Finite Element Method. These performances do not depend on parameters C_b or σ, but only of the mesh size.

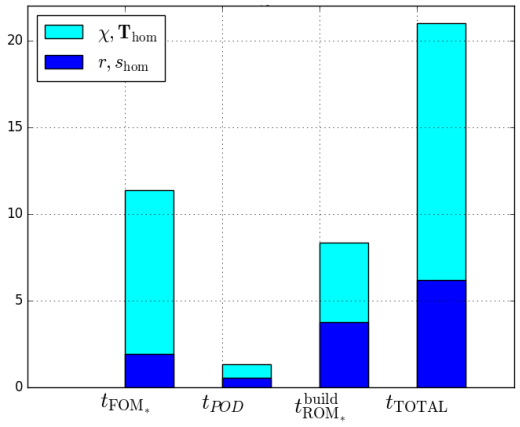

Fig. 11: Time elapsed during the ROM construction

Finally figure 11 shows the time elapsed during the ROM construction. The unity is the mean time of a snapshot computation using the Finite Element Method. The performances involving only the Poisson-Boltzmann equation and the integral s^{hom} of the Boltzmann factor are figures in dark blue, the rest is in light blue. It can be seen that the computation of the snapshots of $\boldsymbol{\chi}$ and its POD-ROM construction takes the most of the time, it due to the fact that the Finite Element space of vetor field $\boldsymbol{\chi}$ has more degrees of freedom than the one containing the scalar field r. To conclude, the use of the ROM for this tridimentional problem is efficient when the number of Cell problems to be solved is greater than 20.

4.2 Multiple inclusions with various parameters

We now focus on a 2D elementary cell with 8 circular inclusions parametrized by two radii ρ_1 and ρ_2 (see figure 12). These two radii correspond respectively to the inclusions numbered 1 and 2 on subfigures 12a and 12b. Furthermore, the variation of the radii of the eight solid inclusions is determined by the pair $(\rho_1,\ \rho_2)$. Indeed, radii of the inclusions 3, 5 and 7 represented on subfigure 12a vary proportionnally to ρ_1, although with different amplitudes, as well as radii of the inclusions 4, 6 and 8 represented by subfigure 12b, vary proportionnaly to ρ_2.

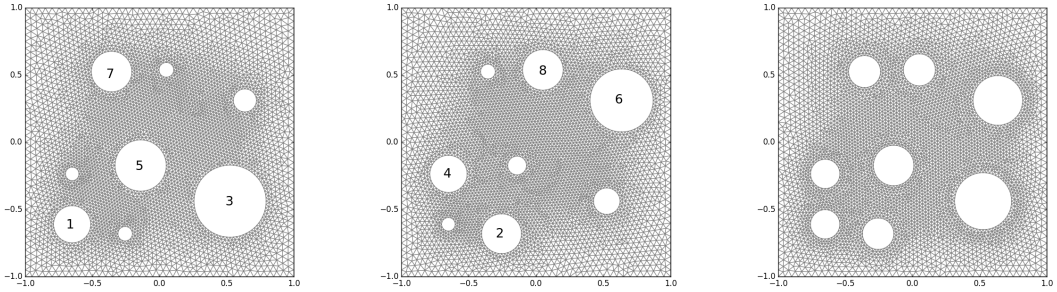

(a) $(\rho_1,\ \rho_2) = (0.1387,\ 0.0547)$ (b) $(\rho_1,\ \rho_2) = (0.0511,\ 0.1485)$ (c) $(\rho_{\star,1}, \rho_{\star,2}) = (0.109,\ 0.109)$

Fig. 12: Meshes for two different Elementary Cells (subigures 12a–12b), and the reference mesh (subigure 12c)

Figure 13 shows the mesh of the reference fluid domain $\mathrm{Y}_\mathrm{f}^\star$, aside with particular solutions $\varphi_\star$ and $\boldsymbol{\chi}_\star$ computed using Finite Element Method.

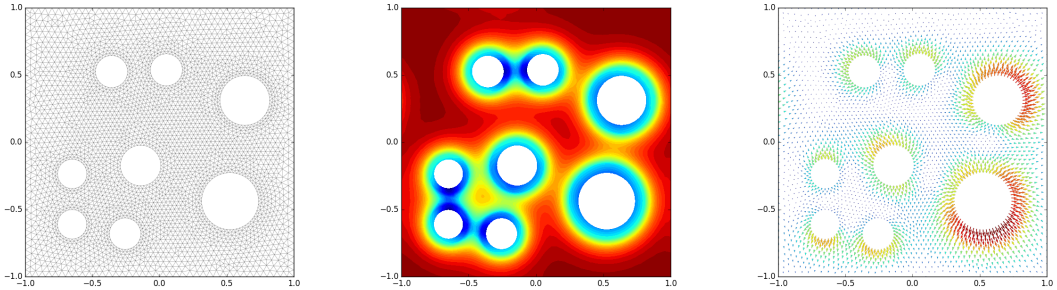

(a) Reference mesh (b) Scalar field $\varphi_\star$ (c) Vector field $\boldsymbol{\chi}_\star$

Fig. 13: Mesh of the reference domain $((\rho_{\star 1},\ \rho_{\star 2}) = (0.1387,\ 0.1385))$ and particular solutions to the cell problems with $(\rho_1,\ \rho_2) = (0.1387,\ 0.1385)$

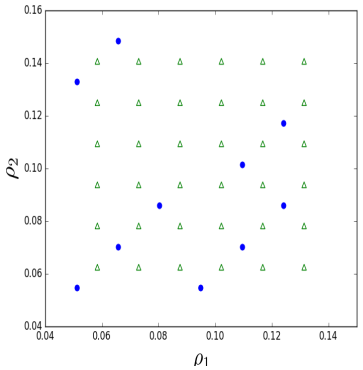

(a) 10 snapshots : Halton sequence

Fig. 14: $(\rho_1,\ \rho_2)$ pairs used for the snapshots computation (blue disks) and for ROM model resolution (green triangles).

The numerical application has been done a set of 10 snapshots. This set corresponds to the parameter values $(\rho_1,\ \rho_2)$ that have been sampled using the Halton sequence method (blue disks, see figure 14a). The reduced order model has been then evaluated for 36 values of $(\rho_1,\ \rho_2)$, represented by the green triangles on figure 14.

In all numerical applications, the following values of the physical parameters are used: $C_\mathrm{b} = 500\,\mathrm{mol.m^{-1}}$ and $\sigma = -0.01\,\mathrm{C.m^{-2}}$. Finally, POD basis $(\phi_l^r)_i$, $(\phi_i^{r^{-1}})_i$ and $(\boldsymbol{\phi}_j)_i$ basis contain 7, 7 and 8 spatial modes, using the energy criterion with $\nu = 10^{-4}$ of POD (99, 999% of representativity). Notice that, since the periodic microstructures involved are no more isotropic (a priori), it is relevant to compute two coefficients, T_{11}^hom and T_{22}^hom (respectively D_{11}^hom and D_{22}^hom), for tensor $\boldsymbol{T}^\mathrm{hom}$ (respectively $\boldsymbol{D}^\mathrm{hom}$).

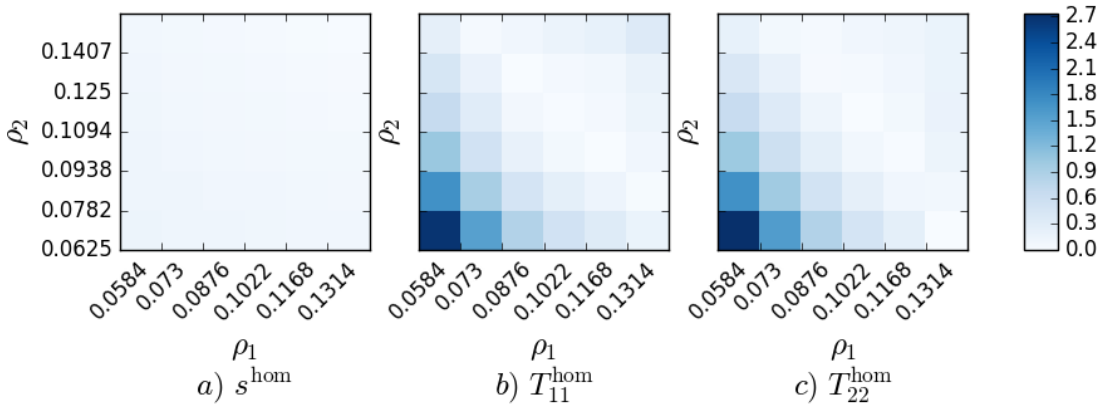

Fig. 15: Relative errors (in percent) between the values of homogenized coefficients obtained by the ROM and those obtained by the FOM.

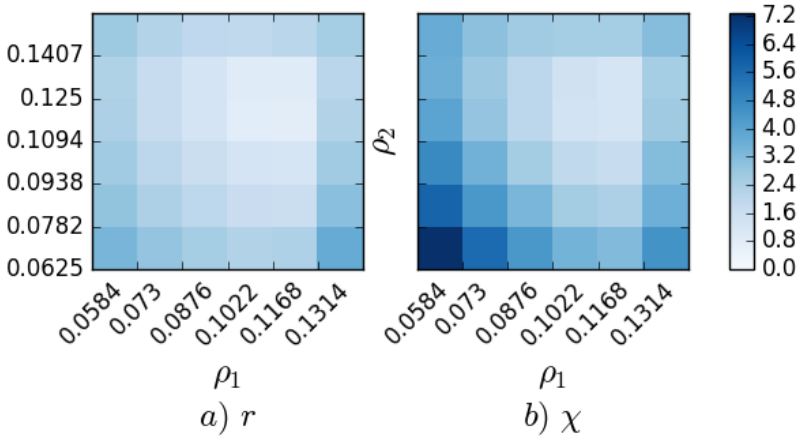

Fig. 16: Relative errors (in percent) between the fields r and $\boldsymbol{\chi}$ obtained by the ROM and those obtained by the FOM.

Figures 15 and 16 represent the ROM estimation errors defined by formulas (69) and (70). ROM errors on s^hom, T_{11}^hom and T_{22}^hom reach at most 0.15% for s^hom, and 2.8% for T_{11}^hom and T_{22}^hom. Moreover, the error is less than 1%, for all coefficients, except for three values of ρ_1, ρ_2 that clearly appear at the bottom left corner of b) and c) subplots of figure 15. The associated ROM errors on fields r and $\boldsymbol{\chi}$ are reached for the smallest values of ρ_1 and ρ_2, they are respectively 3.5% and 7%.

Finally, for these numerical applications to two-dimensional cell problems, the ROM computations have been approximately 100 times faster that those led using the full-order model. An even more important time ratio is expected for three-dimensional cell problems (see figure 10), since the arithmetical complexity of the ROM is independent from the number of degrees of freedom of the full-order model (see [28], section 3.4).

5 Conclusion and perspectives

In this work, we have generalized the approach presented in [28] to solve, in a reduced time, cell problems coming from the periodical homogenization of the Nernst-Planck-Poisson-Boltzmann (NPPB) equations. This approach enables to estimate fastly homogenized tensor coefficients. In [28], the study was limited to cell problems depending only on the fluid phase's geometry, when the Electrical Double Layer (EDL) effects are neglected. At the scale of Debye length, electrodiffusion equations of NPPB, involve the Boltzmann factor $r = e^{-B\varphi}$ associated to the electrical potential φ close to the solid-fluid interface. The POD couldn't be directely performed on potential φ because of the nonlinearity of the NPPB system. To overcome this, a reformulation of NPPB involving the Boltzmann factor r and its inverse u has been proposed, in order to perform the POD-ROM on the three variables r, u and $\boldsymbol{\chi}$. This provided an efficient reduced-order model. The results of this approach have been presented for (i) a three dimensional periodic microstructure consisting of the repetition of a cell with a single spherical, 3D parametrized inclusion, and (ii) a two-dimensional cell with eight circular inclusions, parametrized with two numbers ρ_1 and ρ_2. In the mono-inclusion case, several values of the physical parameters C_b and σ were tested. We have seen that the homogenized coefficient D_{11}^{hom} is restituted with an error below 1% errors in most cases (the error are more important when $\sigma = -0.2\,\mathrm{C.m}^{-2}$ and when the porosity is large). Even for the greatest value of σ tested, the ROM error is less than 10% for low porosities, which are the most realistic for cementitious media. Finally, the time of execution of the ROM is 3 000 times less than when the Finite Element Method is uesd. This ratio only depends on the size of the Finite Element space, and not on the geometrical or physical parameters. In the multi-inclusion case, the Halton sampling method has been used to generate the snapshots, avoiding computing full-order solutions for an important number of parameter values. For all homogenized coeffients, the ROM errors are less than 3% (they are even less than 8% for the solutions r or $\boldsymbol{\chi}$ of the cell problems).

Conflict of interest

The authors declare that they have no conflict of interest.

Acknowledgement

The authors would like to express their sincere thanks to the NEEDS program for having supported this work.

A Galerkin POD-ROM based on the snapshot method

The snapshot method, introduced by Sirovich in [38], was used here to build a Galerkin POD-ROM in order to solve fastly the homogenization cell problem (13) in the case $e^{-B\,\varphi} \simeq 1$. It consists of writing, for all $\boldsymbol{y}$ and $\boldsymbol{\rho}$:

$$\boldsymbol{\chi}(\boldsymbol{y},\boldsymbol{\rho}) \simeq \widehat{\boldsymbol{\chi}}(\boldsymbol{y},\boldsymbol{\rho}) = \sum_{j=1}^{n_{\boldsymbol{\chi}}} a_j(\boldsymbol{\rho})\,\boldsymbol{\phi}_j(\boldsymbol{y})\,, \tag{A.71}$$

where $(\boldsymbol{\phi}_j(\boldsymbol{y}))_j$ is a sequence of space depending fonctions or POD modes.

Firstly, the particular solutions $(\boldsymbol{\chi}(\boldsymbol{y},\boldsymbol{\rho}_j))_j$ of the full-order problem are computed for a set $\{\boldsymbol{\rho}_j\}_{j=1}^{n_{\mathrm{snap}}}$ of values of parameter $\boldsymbol{\rho}$. Then, the POD modes are computed using the formula:

$$\boldsymbol{\phi}_i(\boldsymbol{y}) = \frac{1}{\sqrt{\lambda_i}} \sum_{j=1}^{n_{\mathrm{snap}}} [\boldsymbol{v}_i]_j \boldsymbol{\chi}(\boldsymbol{y},\boldsymbol{\rho}_j)\,, \tag{A.72}$$

where $(\boldsymbol{v}_i)_i$ (respectively $(\lambda_i)_i$) are the unit eigenvectors (respcetively their associated eigenvalues) of the symmetric positive definite correlation matrix:

$$[\boldsymbol{C}^{\boldsymbol{\chi}}]_{ij} = \int_{\mathrm{Y}} \boldsymbol{\chi}(\boldsymbol{y},\boldsymbol{\rho}_i)\cdot\boldsymbol{\chi}(\boldsymbol{y},\boldsymbol{\rho}_j)\,\mathrm{dY}\,. \tag{A.73}$$

Afterwards, the POD basis which appears in the decomposition (A.71) is obtained by retaining the $n_{\boldsymbol{\chi}}$ first vectors of basis $(\boldsymbol{\phi}_i)_i$, where $n_{\boldsymbol{\chi}}$ verifies[6]:

$$n_{\boldsymbol{\chi}} = \min \left\{ n \in 1, \dots, n_{\text{snap}} \;\middle|\; \frac{\sum_{i=1}^{n_{\boldsymbol{\chi}}} \lambda_i}{\sum_{i=1}^{n_{\text{snap}}} \lambda_i} < 1 - \nu \right\} \tag{A.74}$$

where the POD modes have been preliminary sorted so that the λ_i sequence decreases and where ν represents the relative content of information that is eliminated by the POD truncation, chosen prior to the POD basis construction. Since in applications to Mechanics, notably to Fluid Mechanics, threshold ν is of the dimension of an energy, this criterion of selection of the most representative POD modes is called an energy criterion. Thus, the efficiency of the method relies on a good tradeoff between two competing objectives: a small value of ν (for accuracy) and a small number $n_{\boldsymbol{\chi}}$ of POD modes (for CPU and memory consumption low costs).

Then, the Galerkin projection is applied. For example, for the homogenization of the Cell Problem with $e^{-B\varphi}$, the weak form used for the Finite Element resolution is:

$$\int_{\mathrm{Y_f}} \nabla_{\boldsymbol{y}} \boldsymbol{\chi} \colon \nabla_{\boldsymbol{y}} \boldsymbol{v} \mathrm{dY} = -\int_{\mathrm{S_{sf}}} \boldsymbol{v} \cdot \boldsymbol{n} \mathrm{dS} \quad \forall \boldsymbol{v} \tag{A.75}$$

The Galerkin projection consists of injecting the decomposition (A.71) into (A.75), which gives:

$$\sum_{j=1}^{n_{\boldsymbol{\chi}}} a_j(\boldsymbol{\rho}) \int_{\mathrm{Y_f}} \nabla_{\boldsymbol{y}} \boldsymbol{\phi}_j(\boldsymbol{y}) \colon \nabla_{\boldsymbol{y}} \boldsymbol{\phi}_l \mathrm{dY} = -\int_{\mathrm{S_{sf}}} \boldsymbol{\phi}_l \cdot \boldsymbol{n} \mathrm{dS} \quad \forall l \tag{A.76}$$

where mode $\boldsymbol{\phi}_l$ has been taken in place of the test function $\boldsymbol{v}$. Equation (A.76), whose solutions are the $a_j(\boldsymbol{\rho})$, is a set of algebraic equation of size $n_{\boldsymbol{\chi}}$. In practise, its order $n_{\boldsymbol{\chi}}$ is small, thus problem (A.76) is called the Reduced-Order Model of (A.75). It is solved much faster than the original discretized cell problem.

B Geometry-dependent POD-ROM

In order to address the issue of the correlation tensor's definition evoked in section 2.3.2, the authors of [28] have proposed an approach which consists of transporting, for each individual geometrical parameter $\boldsymbol{\rho}$, the cell problem set on $\mathrm{Y_f}(\boldsymbol{\rho})$ on a single reference fluid domain $\mathrm{Y_f^\star}$. This is done by constructing, for each value $\boldsymbol{\rho}$ of the geometrical parameter, a map $\widehat{\boldsymbol{\tau_\rho}}$ which sends $\mathrm{Y_f^\star}$ diffeomorphically onto $\mathrm{Y_f}(\boldsymbol{\rho})$.

B.1 Construction of a transformation

Let $\mathrm{Y} = [-1,1]^d$, $d = 2$ be an elementary cell which consists of a path-wise connected fluid phase, and n_s non-overlapping ball-shaped solid inclusions $\mathrm{Y_{s,}}_n(\rho_n) = \mathcal{B}(\boldsymbol{y}_n, \rho_n)$, $1 \leq n \leq n_\mathrm{s}$. Thus the Elementary Cell's geometry is entirely determined by the set of radii $(\rho_n)_n$ for $1 \leq n \leq n_\mathrm{s}$, which are the geometrical parameters. We denote the set of balls centers $\left\{\boldsymbol{y}_n\right\}_{1\leq n\leq n_\mathrm{s}}$ and the vector of balls radii $\boldsymbol{\rho} = (\rho_n)_{1\leq n\leq n_\mathrm{s}}$. Thus $\mathrm{Y_f} = \mathrm{Y} \setminus \left(\bigcup_{n=1}^{n_\mathrm{s}} \mathrm{Y_{s,}}_n(\rho_n)\right)$ is the Elementary Cell's fluid phase, and $\Gamma_n(\rho_n)$, $1 \leq n \leq n_\mathrm{s}$ its solid-fluid, disconnected interfaces (see figure 17).

The reference domain $\mathrm{Y}^\star$ is the union of the following subdomains:

- $\mathrm{Y_{s,}}_n^\star = \mathcal{B}(\boldsymbol{\xi}_n, \rho_\star)$ the reference solid inclusions centered at $\boldsymbol{\xi}_n = \boldsymbol{y}_n$ all with same reference radius $\rho_\star$,
- $\mathrm{Y_{c,}}_n^\star = \mathcal{B}(\boldsymbol{\xi}_n, q_n) \setminus \mathrm{Y_{s,}}_n^\star$ the crowns around the solid inclusions each with exterior radius q_n and interior radius $\rho_\star$,
- $\mathrm{Y_e^\star} = \mathrm{Y}^\star \setminus \bigcup_{n=1}^{n_\mathrm{s}} (\mathrm{Y_{s,}}_n^\star \cup \mathrm{Y_{c,}}_n^\star)$ the remaining fluid domain exterior to $\bigcup_{n=1}^{n_\mathrm{s}} \mathrm{Y_{c,}}_n^\star$.

[6] Thus $n_{\boldsymbol{\chi}} < n_{\text{snap}}$.

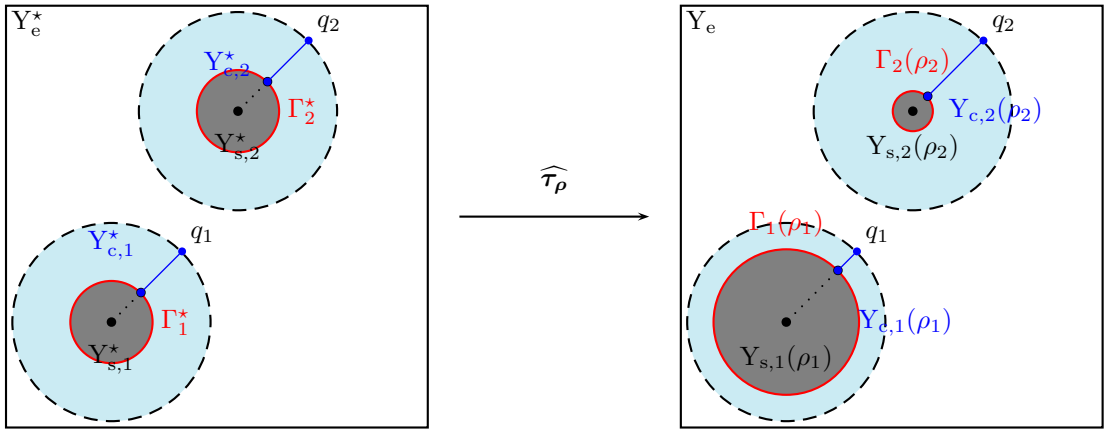

Fig. 17: Transformation $\widehat{\boldsymbol{\tau}_{\boldsymbol{\rho}}}\colon \mathrm{Y}^\star \overset{\boldsymbol{\xi}\mapsto\widehat{\boldsymbol{\tau}_{\boldsymbol{\rho}}}(\boldsymbol{\xi})=\boldsymbol{y}}{\longrightarrow} \mathrm{Y}(\boldsymbol{\rho})$: case of $n_\mathrm{s}=2$ inclusions.

According to figure 17, $\widehat{\boldsymbol{\tau}_{\boldsymbol{\rho}}}$ moves only the points of the fluid phase lying in the crowns around the solid inclusions. It is computed with the explicit formula:

$$\widehat{\boldsymbol{\tau}_{\boldsymbol{\rho}}}(\boldsymbol{\xi}) = \begin{cases} \alpha_{\rho_n}\boldsymbol{u}(\boldsymbol{\xi}-\boldsymbol{\xi}_n)+\beta_{\rho_n}(\boldsymbol{\xi}-\boldsymbol{\xi}_n), & \text{if } \boldsymbol{\xi}\in \mathrm{Y}^\star_{\mathrm{c},n},\ \text{for}\ \ 1\le n\le n_\mathrm{s}, \\ \boldsymbol{\xi}, & \text{if } \boldsymbol{\xi}\in \overline{\mathrm{Y}^\star_\mathrm{e}}, \end{cases} \tag{B.77}$$

where

$$\alpha_{\rho_n} = q_n\frac{\rho_n-\rho_\star}{q_n-\rho_\star}, \quad \beta_{\rho_n} = \frac{q_n-\rho_n}{q_n-\rho_\star}. \tag{B.78}$$

Its inverted is of the same form and is written:

$$\widehat{\boldsymbol{\tau}_{\boldsymbol{\rho}}}^{-1}(\boldsymbol{y}) = \begin{cases} \dfrac{1}{\beta_{\rho_n}}(\boldsymbol{y}-\boldsymbol{y}_n)+\dfrac{\alpha_{\rho_n}}{\beta_{\rho_n}}\dfrac{\boldsymbol{y}-\boldsymbol{y}_n}{\|\boldsymbol{y}-\boldsymbol{y}_n\|}, & \text{if } \boldsymbol{\xi}\in \mathrm{Y}_{\mathrm{c},n},\ \text{for}\ \ 1\le n\le n_\mathrm{s}, \\ \boldsymbol{y}, & \text{if } \boldsymbol{y}\in \overline{\mathrm{Y}^\star_\mathrm{e}}, \end{cases} \tag{B.79}$$

In order to rewrite on $\mathrm{Y}^\star_\mathrm{f}$ the cell problem set on $\mathrm{Y}_\mathrm{f}(\boldsymbol{\rho})$, the Jacobian matrix $\widehat{\boldsymbol{J}_{\boldsymbol{\rho}}}(\boldsymbol{\xi})$, its inverse $\widehat{\boldsymbol{J}_{\boldsymbol{\rho}}}^{-1}(\boldsymbol{\xi})$ and the Jacobian determinant $\widehat{j_{\boldsymbol{\rho}}}(\boldsymbol{\xi})$ for all spatial coordinates $\boldsymbol{\xi}$ an every value $\boldsymbol{\rho}$ of the geometrical parameter. This is easily done through the (B.77)–(B.79) formulas and results in:

$$\widehat{\boldsymbol{J}_{\boldsymbol{\rho}}}(\boldsymbol{\xi}) = \begin{cases} \beta_{\rho_n}\boldsymbol{I}+\alpha_{\rho_n}\dfrac{1}{\|\boldsymbol{\xi}-\boldsymbol{\xi}_n\|}\boldsymbol{G}_{\boldsymbol{u}(\boldsymbol{\xi}-\boldsymbol{\xi}_n)}, & \text{if } \boldsymbol{\xi}\in \mathrm{Y}^\star_{\mathrm{c},n},\ \text{for}\ \ 1\le n\le n_\mathrm{s}, \\ \boldsymbol{I}, & \text{if } \boldsymbol{\xi}\in \overline{\mathrm{Y}^\star_\mathrm{e}}, \end{cases} \tag{B.80}$$

where $\boldsymbol{G}_{\boldsymbol{u}(\boldsymbol{\xi}-\boldsymbol{\xi}_n)} = \boldsymbol{I}-\dfrac{(\boldsymbol{\xi}-\boldsymbol{\xi}_n)\otimes(\boldsymbol{\xi}-\boldsymbol{\xi}_n)}{\|\boldsymbol{\xi}-\boldsymbol{\xi}_n\|^2}$, and

$$\widehat{\boldsymbol{J}_{\boldsymbol{\rho}}}^{-1}(\boldsymbol{\xi}) = \begin{cases} \dfrac{1}{\beta_{\rho_n}}\Big(\boldsymbol{I}-\alpha_{\rho_n}\dfrac{1}{\beta_{\rho_n}\|\boldsymbol{\xi}-\boldsymbol{\xi}_n\|+\alpha_{\rho_n}}\boldsymbol{G}_{\boldsymbol{u}(\boldsymbol{\xi}-\boldsymbol{\xi}_n)}\Big), & \text{if } \boldsymbol{\xi}\in \mathrm{Y}^\star_{\mathrm{c},n},\ \text{for}\ \ 1\le n\le n_\mathrm{s}, \\ \boldsymbol{I}, & \text{if } \boldsymbol{\xi}\in \overline{\mathrm{Y}^\star_\mathrm{e}}. \end{cases} \tag{B.81}$$

B.2 Pulling-back through the parametrized transformation

For all $\boldsymbol{\rho}$, the Elementary Cell problem without EDL effects, whose weak form is:

$$\int_{\mathrm{Y}_\mathrm{f}(\rho)} \nabla_{\boldsymbol{y}}\boldsymbol{\chi} : \nabla_{\boldsymbol{y}}\boldsymbol{v}\,\mathrm{dY} = -\sum_{n=1}^{n_\mathrm{s}}\int_{\Gamma_n(\rho)} \boldsymbol{n}\cdot\boldsymbol{v}\,\mathrm{dS}(\rho)\,, \tag{B.82}$$

is pulled-back, through $\widehat{\boldsymbol{\tau}_{\boldsymbol{\rho}}}^{-1}$, on the reference domain $\mathrm{Y}^\star$. To do this, the vector field $\boldsymbol{\chi}$ is written:

$$\boldsymbol{\chi}(\boldsymbol{y}) = \boldsymbol{\chi}_\star(\widehat{\boldsymbol{\tau}_{\boldsymbol{\rho}}}^{-1}(\boldsymbol{y}))\,, \tag{B.83}$$

and the chain rule[7] is applied, providing:

$$\nabla_{\boldsymbol{y}}\,\boldsymbol{\chi}(\boldsymbol{y}) = \nabla_{\boldsymbol{\xi}=\widehat{\boldsymbol{\tau}_{\boldsymbol{\rho}}}^{-1}\,\boldsymbol{y}}\,\boldsymbol{\chi}_\star\cdot\nabla_{\boldsymbol{y}}\,\widehat{\boldsymbol{\tau}_{\boldsymbol{\rho}}}^{-1}\,, \tag{B.84}$$

[7] Here, $\nabla_{\boldsymbol{y}}\,\boldsymbol{v}$ denotes the spatial derivative $\dfrac{\partial \boldsymbol{v}}{\partial \boldsymbol{y}}$ of the vector field $\boldsymbol{v}$. The gradient of $\boldsymbol{v}$ is then $\big(\nabla_{\boldsymbol{y}}\,\boldsymbol{v}\big)^\intercal$.

and then, through the identity $\nabla_{\boldsymbol{y}}\,\widehat{\boldsymbol{\tau_\rho}}^{-1}(\boldsymbol{y}) = \left(\nabla_{\boldsymbol{\xi}}\,\widehat{\boldsymbol{\tau_\rho}}(\boldsymbol{\xi})\right)^{-1} = \widehat{\boldsymbol{J_\rho}}^{-1}$:

$$\nabla_{\boldsymbol{y}}\,\boldsymbol{\chi}(\boldsymbol{y}) = \nabla_{\boldsymbol{\xi}}\,\boldsymbol{\chi}_\star \cdot \widehat{\boldsymbol{J_\rho}}^{-1}\,. \tag{B.85}$$

Finally, pulling back the expressions $\int_{\mathrm{Y_f}(\rho)}\mathrm{dY}$ and $\int_{\Gamma_n(\rho)}\boldsymbol{n}\cdot\mathrm{dS}(\rho)$ involve the mutiplication of the integrands by the jacobian determinant $\widehat{j_{\boldsymbol{\rho}}}$ and by the interfaces curvatures ratio $g_{\rho,n}$ respectively. Hence, the variational problem (B.82) is rewritten:

$$\int_{\mathrm{Y_f^\star}}\left(\nabla_{\boldsymbol{\xi}}\boldsymbol{\chi}_\star\cdot\widehat{\boldsymbol{J_\rho}}^{-1}\right):\left(\nabla_{\boldsymbol{\xi}}\boldsymbol{v}_\star\cdot\widehat{\boldsymbol{J_\rho}}^{-1}\right)\widehat{j_{\boldsymbol{\rho}}}\,\mathrm{dY}^\star = -\int\limits_{\mathrm{S_{sf}}^\star}\boldsymbol{n}\cdot\boldsymbol{v}_\star\,g_{\boldsymbol{\rho}}\,\mathrm{dS_{sf}}^\star, \tag{B.86}$$

or equivalently:

$$\sum_{n=1}^{n_\mathrm{s}}\int_{\mathrm{Y_{c,}}n^\star}\left(\nabla_{\boldsymbol{\xi}}\boldsymbol{\chi}_\star\cdot\widehat{\boldsymbol{J_\rho}}^{-1}\right):\left(\nabla_{\boldsymbol{\xi}}\boldsymbol{v}_\star\cdot\widehat{\boldsymbol{J_\rho}}^{-1}\right)\widehat{j_{\boldsymbol{\rho}}}\,\mathrm{dY}^\star + \int_{\mathrm{Y_e^\star}}\left(\nabla_{\boldsymbol{\xi}}\boldsymbol{\chi}_\star\right):\nabla_{\boldsymbol{\xi}}\boldsymbol{v}_\star\,\mathrm{dY}^\star = -\sum_{n=1}^{n_\mathrm{s}}\int\limits_{\Gamma_n^\star}\boldsymbol{n}\cdot\boldsymbol{v}_\star\,g_{\rho,n}\,\mathrm{d}\Gamma_n^\star, \tag{B.87}$$

In expression (B.87), the integrals on the reference cell's subdomains $\mathrm{Y_e^\star}$, $\mathrm{Y_{c,}}n^\star$ and $\Gamma_n^\star$ for $1\leq n\leq n_\mathrm{s}$ are written separately. The consequences on model order reduction are explained in the annex B.3. The same approach can be used with the corresponding homogenized tensor $\boldsymbol{D}^{\mathrm{hom}}(\boldsymbol{\rho})$:

$$\boldsymbol{D}^{\mathrm{hom}}(\boldsymbol{\rho}) = D\left(\frac{|\mathrm{Y_f^\star}|}{|\mathrm{Y}^\star|}\boldsymbol{I} + \sum_{n=1}^{n_\mathrm{s}}\int_{\mathrm{Y_{c,}}n^\star}\left(\nabla_{\boldsymbol{\xi}}\boldsymbol{\chi}_\star\cdot\widehat{\boldsymbol{J_\rho}}^{-1}\right)^\intercal\widehat{j_{\boldsymbol{\rho}}}\,\mathrm{dY}^\star + \int_{\mathrm{Y_e^\star}}\nabla_{\boldsymbol{\xi}}\boldsymbol{\chi}_\star^\intercal\,\mathrm{dY}^\star\right), \tag{B.88}$$

This generalizes with no difficulty to the case when the EDL effects are taken into account, provided the relation:

$$\nabla_{\boldsymbol{y}}\,r = \left(\frac{\partial r}{\partial\boldsymbol{y}}\right)^\intercal = \left(\frac{\partial r_\star}{\partial\boldsymbol{\xi}}(\widehat{\boldsymbol{\tau_\rho}}(\boldsymbol{\xi}))\circ\widehat{\boldsymbol{J_\rho}}^{-1}\right)^\intercal = \widehat{\boldsymbol{J_\rho}}^{-\intercal}\,\nabla_{\boldsymbol{\xi}}\,r_\star(\boldsymbol{\xi})\,. \tag{B.89}$$

involving the scalar field $r = e^{-B\,\varphi}$.

B.3 Affine dependency in the parameters

POD-ROM efficiency relies on the possibility to compute expressions involving $\widehat{j_{\boldsymbol{\rho}}}$, $\widehat{\boldsymbol{J_\rho}}^{-1}\,\widehat{j_{\boldsymbol{\rho}}}$, $\widehat{\boldsymbol{J_\rho}}^{-2}\,\widehat{j_{\boldsymbol{\rho}}}$ and $g_{\rho,n}$. for any given $\boldsymbol{\rho}$. This is done by separating the integration variable $\boldsymbol{\xi}$ from the geometrical parameter $\boldsymbol{\rho}$ in each of these expreaaions: this is the so-called affine dependency on the parameters verified by the four expressions above.

Firstly, an explicit formula for the Jacobian determinant is found by the diagonalization of the matrices that appear in equation (B.80). Indeed, $\boldsymbol{G}_{\boldsymbol{u}(\boldsymbol{\xi}-\boldsymbol{\xi}_n)}$ is a projection matrix and this leads to:

$$\widehat{j_{\boldsymbol{\rho}}}(\boldsymbol{\xi}) = \begin{cases}\displaystyle\sum_{p=0}^{d-1}\frac{C_{d-1}^p\,\alpha_{\rho_n}^p\,\beta_{\rho_n}^{d-p}}{\|\,\boldsymbol{\xi}-\boldsymbol{\xi}_n\,\|^p} = \beta_{\rho_n}\,\frac{\left(\beta_{\rho_n}\|\boldsymbol{\xi}-\boldsymbol{\xi}_n\|+\alpha_{\rho_n}\right)^{d-1}}{\|\boldsymbol{\xi}-\boldsymbol{\xi}_n\|^{d-1}}, & \text{if } \boldsymbol{\xi}\in\mathrm{Y_{c,}}n^\star,\ \text{for}\ \ 1\leq n\leq n_\mathrm{s},\\ 1 & \text{if } \boldsymbol{\xi}\in\overline{\mathrm{Y_e^\star}},\end{cases} \tag{B.90}$$

For this reason, the left-hand side of equation (B.87) is splitted into integrals computed over the fluid subdomains $\overline{\mathrm{Y_e^\star}}$, and $\mathrm{Y_{c,}}n^\star$ for $1\leq n\leq n_\mathrm{s}$.

It is remarkable that the expression upside (B.90) depends on the dimension $d=2$, 3 of the elementary cell. Consequently, this is also the case of expressions $\widehat{\boldsymbol{J_\rho}}^{-1}\,\widehat{j_{\boldsymbol{\rho}}}$ and $\widehat{\boldsymbol{J_\rho}}^{-2}\,\widehat{j_{\boldsymbol{\rho}}}$. In [28], the authors proved that, in dimension $d=3$:

$$\begin{aligned}\left(\widehat{\boldsymbol{J_\rho}}^{-1}\right)\widehat{j_{\boldsymbol{\rho}}} = &\left(\beta_{\rho_n}^2 + 2\alpha_{\rho_n}\beta_{\rho_n}\frac{1}{\|\boldsymbol{\xi}-\boldsymbol{\xi}_n\|} + \alpha_{\rho_n}^2\frac{1}{\|\boldsymbol{\xi}-\boldsymbol{\xi}_n\|^2}\right)\boldsymbol{I}\\ &-\alpha_{\rho_n}\beta_{\rho_n}\frac{1}{\|\boldsymbol{\xi}-\boldsymbol{\xi}_n\|}\,\boldsymbol{G}_{\boldsymbol{u}(\boldsymbol{\xi}-\boldsymbol{\xi}_n)} - \alpha_{\rho_n}^2\frac{1}{\|\boldsymbol{\xi}-\boldsymbol{\xi}_n\|^2}\,\boldsymbol{G}_{\boldsymbol{u}(\boldsymbol{\xi}-\boldsymbol{\xi}_n)}\,,\end{aligned} \tag{B.91}$$

and

$$\begin{aligned}\left(\widehat{\boldsymbol{J_\rho}}^{-2}\right)\widehat{j_{\boldsymbol{\rho}}} = &\left(\beta_{\rho_n} + \frac{2\alpha_{\rho_n}}{\|\boldsymbol{\xi}-\boldsymbol{\xi}_n\|} + \frac{\alpha_{\rho_n}^2}{\beta_{\rho_n}\|\boldsymbol{\xi}-\boldsymbol{\xi}_n\|^2}\right)\boldsymbol{I}\\ &-\frac{2\alpha_{\rho_n}}{\|\boldsymbol{\xi}-\boldsymbol{\xi}_n\|}\boldsymbol{G}_{\boldsymbol{u}(\boldsymbol{\xi}-\boldsymbol{\xi}_n)} - \frac{\alpha_{\rho_n}^2}{\beta_{\rho_n}\|\boldsymbol{\xi}-\boldsymbol{\xi}_n\|^2}\boldsymbol{G}_{\boldsymbol{u}(\boldsymbol{\xi}-\boldsymbol{\xi}_n)}\,.\end{aligned} \tag{B.92}$$

If $\boldsymbol{\xi}\in\mathrm{Y_{c,}}n^\star$, for $1\leq n\leq n_\mathrm{s}$. For two-dimensional Elementary Cells ($d=2$), [28] provides a truncated decomposition of $\widehat{\boldsymbol{J_\rho}}^{-2}\,\widehat{j_{\boldsymbol{\rho}}}$:

$$\begin{aligned}\widehat{\boldsymbol{J}_{\boldsymbol{\rho}}}^{-2}\widehat{j_{\boldsymbol{\rho}}} \simeq & \left(1+\frac{\alpha_{\rho_n}}{\beta_{\rho_n}\|\boldsymbol{\xi}-\boldsymbol{\xi}_n\|}\right)\boldsymbol{I} \\ & -\left(1+\beta_{\rho_n}^{N_{\rm dev}+1}\right)\frac{\alpha_{\rho_n}}{\beta_{\rho_n}\|\boldsymbol{\xi}-\boldsymbol{\xi}_n\|}\cdot\boldsymbol{G}_{\boldsymbol{u}(\boldsymbol{\xi}-\boldsymbol{\xi}_n)} \\ & +\sum_{p=1}^{N_{\rm dev}}(-1)^p\left(\sum_{m=p}^{N_{\rm dev}}\beta_{\rho_n}^m C_m^p\right)(1-\beta_{\rho_n})\frac{\alpha_{\rho_n}}{\beta_{\rho_n}q^p}\|\boldsymbol{\xi}-\boldsymbol{\xi}_n\|^{p-1}\boldsymbol{G}_{\boldsymbol{u}(\boldsymbol{\xi}-\boldsymbol{\xi}_n)}\end{aligned} \tag{B.93}$$

when $\boldsymbol{\xi}\in \mathrm{Y}^\star_{\mathrm{c},n}$ for $1\le n\le n_{\rm s}$, and $\widehat{\boldsymbol{J}_{\boldsymbol{\rho}}}^{-2}\widehat{j_{\boldsymbol{\rho}}}=\boldsymbol{I}$ elsewhere (in practice $N_{\rm dev}=2$ gives a good approximation). Furthermore $\widehat{\boldsymbol{J}_{\boldsymbol{\rho}}}^{-1}\widehat{j_{\boldsymbol{\rho}}}$ admits, when $d=2$, the exact decomposition:

$$\widehat{\boldsymbol{J}_{\boldsymbol{\rho}}}^{-1}\widehat{j_{\boldsymbol{\rho}}}=\begin{cases}\left(\beta_{\rho_n}+\alpha_{\rho_n}\frac{1}{\|\boldsymbol{\xi}-\boldsymbol{\xi}_n\|}\right)\boldsymbol{I}-\alpha_{\rho_n}\dfrac{1}{\|\boldsymbol{\xi}-\boldsymbol{\xi}_n\|}\boldsymbol{G}_{\boldsymbol{u}(\boldsymbol{\xi}-\boldsymbol{\xi}_n)} & \text{if } \boldsymbol{\xi}\in \mathrm{Y}^\star_{\mathrm{c},n},\ \text{for}\ \ 1\le n\le n_{\rm s},\\ \boldsymbol{I} & \text{if } \boldsymbol{\xi}\in\overline{\mathrm{Y}^\star_{\mathrm{e}}},\end{cases} \tag{B.94}$$

Finally, variables $\boldsymbol{\xi}$ and $\boldsymbol{\rho}$ are separated in the integrals over the interfaces $\Gamma^\star_n$, $1\le n\le n_{\rm s}$. This is done by writing for all n and vector field $\boldsymbol{v}$:

$$\int_{\mathrm{S}_{\rm sf}}\boldsymbol{n}\cdot\boldsymbol{v}\,\mathrm{d}\Gamma_n=\int_{\Gamma^\star_n}\boldsymbol{v}_\star\cdot j_{\rho_n}\left((\boldsymbol{J}_{\rho_n})^{-\intercal}\,\boldsymbol{n}_\star(\boldsymbol{\xi})\right)\mathrm{d}\boldsymbol{\xi}=\int_{\Gamma^\star_n}\boldsymbol{v}_\star\cdot j_{\rho_n}\left((\boldsymbol{J}_{\rho_n})^{-1}\,\frac{\boldsymbol{\xi}-\boldsymbol{\xi}_n}{\|\boldsymbol{\xi}-\boldsymbol{\xi}_n\|}\right)\mathrm{d}\boldsymbol{\xi}\,, \tag{B.95}$$

since $\boldsymbol{J}_{\rho_n}$ is symmetric. Furthermore:

$$(\boldsymbol{J}_{\rho_n}(\boldsymbol{\xi}))^{-1}\,(\boldsymbol{\xi}-\boldsymbol{\xi}_n)=\frac{1}{\beta_{\rho_n}}\left(\boldsymbol{\xi}-\boldsymbol{\xi}_n-\alpha_{\rho_n}\frac{1}{\|\boldsymbol{\xi}-\boldsymbol{\xi}_n\|}\left(\boldsymbol{\xi}-\boldsymbol{\xi}_n-\frac{(\boldsymbol{\xi}-\boldsymbol{\xi}_n)\otimes(\boldsymbol{\xi}-\boldsymbol{\xi}_n)}{\|\boldsymbol{\xi}-\boldsymbol{\xi}_n\|^2}\,(\boldsymbol{\xi}-\boldsymbol{\xi}_n)\right)\right)=\frac{1}{\beta_{\rho_n}}\,(\boldsymbol{\xi}-\boldsymbol{\xi}_n)\,. \tag{B.96}$$

This, combined with relation $j_{\rho_n}=\beta_{\rho_n}\dfrac{\|\widehat{\boldsymbol{\tau}_{\boldsymbol{\rho}}}(\boldsymbol{\xi}-\boldsymbol{\xi}_n)\|^{d-1}}{\|\boldsymbol{\xi}-\boldsymbol{\xi}_n\|^{d-1}}$, provides:

$$\int_{\Gamma^\star_n}\boldsymbol{v}_\star\cdot j_{\rho_n}\left((\boldsymbol{J}_{\rho_n})^{-1}\,\frac{\boldsymbol{\xi}-\boldsymbol{\xi}_n}{\|\boldsymbol{\xi}-\boldsymbol{\xi}_n\|}\right)\mathrm{d}\boldsymbol{\xi}=\int_{\Gamma^\star_n}\boldsymbol{v}_\star\cdot\frac{\boldsymbol{\xi}-\boldsymbol{\xi}_n}{\|\boldsymbol{\xi}-\boldsymbol{\xi}_n\|}\,\frac{\|\widehat{\boldsymbol{\tau}_{\boldsymbol{\rho}}}(\boldsymbol{\xi}-\boldsymbol{\xi}_n)\|^{d-1}}{\|\boldsymbol{\xi}-\boldsymbol{\xi}_n\|^{d-1}}\,\mathrm{d}\boldsymbol{\xi}=\int_{\Gamma^\star_n}\boldsymbol{v}_\star\cdot\boldsymbol{n}_\star\,\frac{\rho_n^{d-1}}{{\rho_\star}_n^{d-1}}\,\mathrm{d}\boldsymbol{\xi}\,. \tag{B.97}$$

where the curvature ratio $\left(\dfrac{\rho_n}{\rho_\star}\right)^{d-1}$ of interfaces Γ_n and $\Gamma^\star_n$ appears explicitely. In conclusion, the pullback of $\displaystyle\int_{\mathrm{S}_{\rm sf}}\boldsymbol{n}\cdot\boldsymbol{v}\,\mathrm{d}\Gamma_n$ is simply written

$$\int\limits_{\Gamma^\star_n}\boldsymbol{n}\cdot\boldsymbol{v}_\star\,g_{\rho,n}\,\mathrm{d}\Gamma^\star_n\quad\text{with}\quad g_{\rho,n}=\left(\frac{\rho_n}{\rho_\star}\right)^{d-1}. \tag{B.98}$$

In relation (B.98), variables $\boldsymbol{\rho}$ and $\boldsymbol{\xi}$ are trivially separated.

This concludes the affine decomposition of the expressions involved by the pullback of the cell problems. These decompositions are true, whether or not the EDL effects are taken into account.

C ROM for NPPB

The Galerkin projection of equation (28), recalled here:

$$\int\limits_{\mathrm{Y}^\star_{\rm f}}r_\star(\nabla_{\boldsymbol{\xi}}\boldsymbol{\chi}_\star\,\widehat{\boldsymbol{J}_{\boldsymbol{\rho}}}^{-1})\colon(\nabla_{\boldsymbol{\xi}}\boldsymbol{v}_\star\,\widehat{\boldsymbol{J}_{\boldsymbol{\rho}}}^{-1})\,\widehat{j_{\boldsymbol{\rho}}}\mathrm{d}\mathrm{Y}^\star=\int\limits_{\mathrm{Y}^\star_{\rm f}}\widehat{\boldsymbol{J}_{\boldsymbol{\rho}}}^{-\intercal}\nabla_{\boldsymbol{\xi}}\,r_\star\cdot\boldsymbol{v}_\star\,\widehat{j_{\boldsymbol{\rho}}}\mathrm{d}\mathrm{Y}^\star-\int\limits_{\mathrm{S}_{\rm sf}{}^\star}r_\star\boldsymbol{v}_\star\cdot\boldsymbol{n}_\star\,g_{\boldsymbol{\rho}}\,\mathrm{d}\mathrm{S}^\star\quad\forall\boldsymbol{v}_\star\in V_\star, \tag{C.99}$$

on POD basis $(\phi_i^r(\boldsymbol{\xi}))_{i=1}^{n_r}$ and $(\boldsymbol{\phi}_j(\boldsymbol{\xi}))_{j=1}^{n_{\boldsymbol{\chi}}}$ provides the following ROM for vector field $\boldsymbol{\chi}$:

$$\sum_{j=1}^{n_{\boldsymbol{\chi}}}\sum_{i=1}^{n_r}\boldsymbol{A}^{\boldsymbol{\chi}}_{\boldsymbol{\rho}\,jli}\,b^i(\rho)a^j(\rho)=\sum_{i=1}^{n_r}\boldsymbol{B}^{\boldsymbol{\chi}}_{\boldsymbol{\rho}\,li}b^i(\rho)-\sum_{i=1}^{n_r}\boldsymbol{C}^{\boldsymbol{\chi}}_{\boldsymbol{\rho}\,li}b^i(\rho), \tag{C.100}$$

where:

$$\boldsymbol{A}^{\boldsymbol{\chi}}_{\boldsymbol{\rho}\,jli}=\int_{\mathrm{Y}^\star_{\rm f}}\left(\nabla_{\boldsymbol{\xi}}\boldsymbol{\phi}_j\,\widehat{\boldsymbol{J}_{\boldsymbol{\rho}}}^{-1}\right)\colon\left(\nabla_{\boldsymbol{\xi}}\boldsymbol{\phi}_l\,\widehat{\boldsymbol{J}_{\boldsymbol{\rho}}}^{-1}\right)\,\phi_i^r\,\widehat{j_{\boldsymbol{\rho}}}\,\mathrm{d}\mathrm{Y}^\star=\int\limits_{\mathrm{Y}^\star_{\rm f}}\phi_i^r\,\nabla\,\boldsymbol{\phi}_j\,\widehat{\boldsymbol{J}_{\boldsymbol{\rho}}}^{-2}\,\widehat{j_{\boldsymbol{\rho}}}:\nabla\boldsymbol{\phi}_l\,\mathrm{d}\mathrm{Y}^\star \tag{C.101}$$

$$\boldsymbol{B}^{\boldsymbol{\chi}}_{\boldsymbol{\rho}\,li}=\int_{\mathrm{Y}^\star_{\rm f}}\left(\widehat{\boldsymbol{J}_{\boldsymbol{\rho}}}^{-\intercal}\,\nabla_{\boldsymbol{\xi}}\phi_i^r\right)\cdot\boldsymbol{\phi}_l\,\widehat{j_{\boldsymbol{\rho}}}\,\mathrm{d}\mathrm{Y}^\star=\int\limits_{\mathrm{Y}^\star_{\rm f}}\left(\widehat{\boldsymbol{J}_{\boldsymbol{\rho}}}^{-1}\,\widehat{j_{\boldsymbol{\rho}}}\right)^{\intercal}\nabla\phi_i^r\cdot\boldsymbol{\phi}_l\,\mathrm{d}\mathrm{Y}^\star \tag{C.102}$$

$$\boldsymbol{C}^{\boldsymbol{\chi}}_{\boldsymbol{\rho}\,li}=\int_{\mathrm{S}_{\rm sf}{}^\star}\phi_i^r\,\boldsymbol{n}\cdot\boldsymbol{\phi}_l\,g_{\boldsymbol{\rho}}\,\mathrm{d}\mathrm{S}^\star, \tag{C.103}$$

Samely, the homogenized tensor $\widehat{\boldsymbol{D}}^{\mathrm{hom}}$ coming from the Reduced-Order Model is written according to (30):

$$\widehat{\boldsymbol{D}}^{\mathrm{hom}}(\rho) = \frac{1}{|\mathrm{Y}^\star|}\sum_{i=1}^{n_r} b^i\, \boldsymbol{s}_{\boldsymbol{\rho}\, i}\, \boldsymbol{I} + \frac{1}{|\mathrm{Y}^\star|}\sum_{i=1}^{n_r} b^i \sum_{j=1}^{n_{\boldsymbol{\chi}}} a^j\, \boldsymbol{K}^r_{\boldsymbol{\rho}\, ij}\,, \tag{C.104}$$

where:

$$\boldsymbol{s}_{\boldsymbol{\rho}\, i} = \int_{\mathrm{Y}^\star_{\mathrm{c}}} \phi^r_i\, \widehat{j_{\boldsymbol{\rho}}}\, \mathrm{dY}^\star\,, \tag{C.105}$$

$$\left[\boldsymbol{K}^r_{\boldsymbol{\rho}\, ij}\right]_{ab} = \int_{\mathrm{Y}^\star_{\mathrm{f}}} \phi^r_i \left[\nabla_{\boldsymbol{\xi}}\boldsymbol{\phi}_j\, \widehat{\boldsymbol{J}_{\boldsymbol{\rho}}}^{-1}\right]_{ba} \widehat{j_{\boldsymbol{\rho}}}\, \mathrm{dY}^\star\,. \tag{C.106}$$

According to section B.3, the affine decomposition of integrands in $\boldsymbol{C}^{\boldsymbol{\chi}}_{\boldsymbol{\rho}}$ and $\boldsymbol{s}_{\boldsymbol{\rho}}$ is the same for any dimension of the Cell domain. The coefficients $\boldsymbol{C}^{\boldsymbol{\chi}}_{\boldsymbol{\rho}}$ that appear in the ROM of $\boldsymbol{\chi}$ are thus written:

$$\boldsymbol{C}^{\boldsymbol{\chi}}_{\boldsymbol{\rho}} = \overline{\boldsymbol{C}^{\boldsymbol{\chi}}} + \sum_{n=1}^{n_{\mathrm{s}}} g_{\rho,n}\, [\widetilde{\boldsymbol{C}^{\boldsymbol{\chi}}}_n]_{li}\,, \tag{C.107}$$

where:

$$[\overline{\boldsymbol{C}^{\boldsymbol{\chi}}}]_{li} = \int_{\mathrm{S}_{\mathrm{sf}}{}^\star} \phi^r_i\, \boldsymbol{n}\cdot\boldsymbol{\phi}_l\, \mathrm{dS}^\star, \quad ; \quad [\widetilde{\boldsymbol{C}^{\boldsymbol{\chi}}}_n]_{li} = \int_{\mathrm{S}_{\mathrm{sf}}{}^\star{}_n} \phi^r_i\, \boldsymbol{n}\cdot\boldsymbol{\phi}_l\, g_{\rho,n}\, \mathrm{dS}^\star{}_n \quad \text{and} \quad g_{\rho,n} = \left(\frac{\rho_n}{\rho_{\star\, n}}\right)^{d-1}. \tag{C.108}$$

Moreover, the coefficients $\boldsymbol{s}_{\boldsymbol{\rho}}$ used in the fast computation of $\boldsymbol{D}^{\mathrm{hom}}$ are:

$$\boldsymbol{s}_{\boldsymbol{\rho}} = \overline{\boldsymbol{s}} + \sum_{p=0}^{d-1} C^p_{d-1}\alpha^p_\rho \beta^{d-p}_\rho \widetilde{\boldsymbol{s}}_p \tag{C.109}$$

where:

$$\left[\overline{\boldsymbol{s}}\right]_i = \int_{\mathrm{Y}^\star_{\mathrm{e}}} \phi^r_i\, \mathrm{dY}^\star \quad \text{and} \quad \left[\widetilde{\boldsymbol{s}}_p\right]_i = \int_{\mathrm{Y}^\star_{\mathrm{c}}} \phi^r_i\, \frac{1}{\parallel \boldsymbol{\xi} \parallel^p}\, \mathrm{dY}^\star \tag{C.110}$$

Furthermore, like in the case where the EDL effects are neglected [28], the affine decomposition formulae (B.90)–(B.94) furnish decompositions for $\boldsymbol{A}^{\boldsymbol{\chi}}_{\boldsymbol{\rho}\, jli}$, $\boldsymbol{B}^{\boldsymbol{\chi}}_{\boldsymbol{\rho}\, li}$ and $\boldsymbol{K}^r_{\boldsymbol{\rho}}$, that are different whether the Cell's dimension d id 2 or 3.

Dimension 3

Firstly,

$$\boldsymbol{A}^{\boldsymbol{\chi}}_{\boldsymbol{\rho}} = \overline{\boldsymbol{A}^{\boldsymbol{\chi}}} + \beta_\rho \widetilde{\boldsymbol{A}^{\boldsymbol{\chi}}}_{0,0} + 2\alpha_\rho \widetilde{\boldsymbol{A}^{\boldsymbol{\chi}}}_{1,0} + \frac{\alpha^2_\rho}{\beta_\rho}\widetilde{\boldsymbol{A}^{\boldsymbol{\chi}}}_{2,0} - 2\alpha_\rho \widetilde{\boldsymbol{A}^{\boldsymbol{\chi}}}_{1,1} - \frac{\alpha^2_\rho}{\beta_\rho}\widetilde{\boldsymbol{A}^{\boldsymbol{\chi}}}_{2,1}, \tag{C.111}$$

where:

$$\left[\overline{\boldsymbol{A}^{\boldsymbol{\chi}}}\right]_{jli} = \int_{\mathrm{Y}^\star_{\mathrm{e}}} \phi^r_i \nabla_{\boldsymbol{\xi}}\boldsymbol{\phi}_j : \nabla_{\boldsymbol{\xi}}\boldsymbol{\phi}_l\, \mathrm{dY}^\star, \tag{C.112}$$

$$\left[\widetilde{\boldsymbol{A}^{\boldsymbol{\chi}}}_{p,0}\right]_{jli} = \int_{\mathrm{Y}^\star_{\mathrm{c}}} \phi^r_i \frac{\nabla_{\boldsymbol{\xi}}\boldsymbol{\phi}_j : \nabla_{\boldsymbol{\xi}}\boldsymbol{\phi}_l}{\parallel \boldsymbol{\xi} \parallel^p}\, \mathrm{dY}^\star\,, \text{ for } \; 0 \le p \le d-1, \tag{C.113}$$

$$\left[\widetilde{\boldsymbol{A}^{\boldsymbol{\chi}}}_{p,1}\right]_{jli} = \int_{\mathrm{Y}^\star_{\mathrm{c}}} \phi^r_i \left(\frac{1}{\|\boldsymbol{\xi}\|^p}\, \nabla_{\boldsymbol{\xi}}\boldsymbol{\phi}_j\, \boldsymbol{G}_{\boldsymbol{u}(\boldsymbol{\xi})}\right) : \nabla_{\boldsymbol{\xi}}\boldsymbol{\phi}_l\, \mathrm{dY}^\star\,. \text{ for } \; p \in \{1,2\}\,. \tag{C.114}$$

Furthermore,

$$\boldsymbol{B}^{\boldsymbol{\chi}}_{\boldsymbol{\rho}} = \overline{\boldsymbol{B}^{\boldsymbol{\chi}}} + \beta^2_\rho \widetilde{\boldsymbol{B}^{\boldsymbol{\chi}}}_{0,0} + 2\alpha_\rho\beta_\rho \widetilde{\boldsymbol{B}^{\boldsymbol{\chi}}}_{1,0} + \alpha^2_\rho \widetilde{\boldsymbol{B}^{\boldsymbol{\chi}}}_{2,0} - \alpha_\rho\, \beta_\rho\, \widetilde{\boldsymbol{B}^{\boldsymbol{\chi}}}_{1,1} - \alpha^2_\rho\, \widetilde{\boldsymbol{B}^{\boldsymbol{\chi}}}_{2,1}\,, \tag{C.115}$$

where:

$$\left[\overline{\boldsymbol{B}^{\boldsymbol{\chi}}}\right]_{li} = \int_{\mathrm{Y}^\star_{\mathrm{e}}} \nabla_{\boldsymbol{\xi}}\phi^r_i \cdot \boldsymbol{\phi}_l\, \mathrm{dY}^\star, \tag{C.116}$$

$$\left[\widetilde{\boldsymbol{B}^{\boldsymbol{\chi}}}_{p,0}\right]_{li} = \int_{\mathrm{Y}^\star_{\mathrm{c}}} \frac{\nabla_{\boldsymbol{\xi}}\phi^r_i \cdot \boldsymbol{\phi}_l}{\parallel \boldsymbol{\xi} \parallel^p}\, \mathrm{dY}^\star, \text{ for } \; 0 \le p \le 2, \tag{C.117}$$

$$\left[\widetilde{\boldsymbol{B}^{\boldsymbol{\chi}}}_{p,1}\right]_{li} = \int_{\mathrm{Y}^\star_{\mathrm{c}}} \left(\frac{1}{\parallel \boldsymbol{\xi} \parallel^p} \boldsymbol{G}_{\boldsymbol{u}(\boldsymbol{\xi})}\, \nabla_{\boldsymbol{\xi}}\phi^r_i\right) \cdot \boldsymbol{\phi}_l\, \mathrm{dY}^\star, \text{ for } \; p \in \{1,2\}\,. \tag{C.118}$$

Finally:

$$\boldsymbol{K}^r_{\boldsymbol{\rho}} = \overline{\boldsymbol{K}^r} + \beta^2_\rho \widetilde{\boldsymbol{K}^r}_{(0,0)} + 2\alpha_\rho\beta_\rho \widetilde{\boldsymbol{K}^r}_{(1,0)} + \alpha^2_\rho \widetilde{\boldsymbol{K}^r}_{(2,0)} - \alpha_\rho\, \beta_\rho\, \widetilde{\boldsymbol{K}^r}_{(1,1)} - \alpha^2_\rho\, \widetilde{\boldsymbol{K}^r}_{(2,1)} \tag{C.119}$$

where:

$$\left[\overline{\boldsymbol{K}^r}_{ji}\right]_{ab} = \int_{\mathrm{Y}^\star_{\mathrm{e}}} \phi^r_i\, [\nabla_{\boldsymbol{\xi}}\boldsymbol{\phi}_j]_{ba}\, \mathrm{dY}^\star, \tag{C.120}$$

$$\left[\widetilde{\boldsymbol{K}^r}_{(p,0)\; ji}\right]_{ab} = \int_{\mathrm{Y}^\star_{\mathrm{c}}} \phi^r_i\, [\nabla_{\boldsymbol{\xi}}\boldsymbol{\phi}_j]_{ba} \frac{1}{\parallel \boldsymbol{\xi} \parallel^p}\, \mathrm{dY}^\star, \text{ pour } \; 0 \le p \le 2, \tag{C.121}$$

$$\left[\widetilde{\boldsymbol{K}^r}_{(p,1)\; ji}\right]_{ab} = \int_{\mathrm{Y}^\star_{\mathrm{c}}} \phi^r_i\, [\nabla_{\boldsymbol{\xi}}\boldsymbol{\phi}_j\, \boldsymbol{G}_{\boldsymbol{u}(\boldsymbol{\xi})}]_{ba} \frac{1}{\parallel \boldsymbol{\xi} \parallel^p}\, \mathrm{dY}^\star, \text{ pour } \; p \in \{1,2\} \tag{C.122}$$

Dimension 2

In this case, the decomposition of $\boldsymbol{A}^{\boldsymbol{\chi}}_{\boldsymbol{\rho}}$ cannot be done exactely. The following truncated formula is used:

$$\begin{aligned}\boldsymbol{A}^{\rho} \simeq \overline{\boldsymbol{A}^{\boldsymbol{\chi}}} + \widetilde{\boldsymbol{A}^{\boldsymbol{\chi}}}_{0,0} + \frac{\alpha_\rho}{\beta_\rho}\widetilde{\boldsymbol{A}^{\boldsymbol{\chi}}}_{1,0} - \left(1+\beta_\rho^{N_{\text{dev}}+1}\right)\frac{\alpha_\rho}{\beta_\rho}\widetilde{\boldsymbol{A}^{\boldsymbol{\chi}}}_{0,1} \\ + \sum_{p=1}^{N_{\text{dev}}}(-1)^p\left(\sum_{m=p}^{N_{\text{dev}}}\beta_\rho^m C_m^p\right)(1-\beta_\rho)\frac{\alpha_\rho}{\beta_\rho q^p}\widetilde{\boldsymbol{A}^{\boldsymbol{\chi}}}_{p,1}\end{aligned} \tag{C.123}$$

with previous notation for $\overline{\boldsymbol{A}^{\boldsymbol{\chi}}}$, $\widetilde{\boldsymbol{A}^{\boldsymbol{\chi}}}_{p,0}$ and:

$$\left[\widetilde{\boldsymbol{A}^{\boldsymbol{\chi}}}_{p,1}\right]_{jli} = \int_{\mathrm{Y}_c^\star}\phi_i^r\left(\|\,\boldsymbol{\xi}\,\|^{p-1}\;\nabla_{\boldsymbol{\xi}}\boldsymbol{\phi}_j\,\boldsymbol{G}_{\boldsymbol{u}(\boldsymbol{\xi})}\right):\nabla_{\boldsymbol{\xi}}\boldsymbol{\phi}_l\,\mathrm{d}\mathrm{Y}^\star\,,\text{for}\;\;p=0\,,\ldots\,,N_{\text{dev}}\,. \tag{C.124}$$

$\boldsymbol{B}^{\boldsymbol{\chi}}_{\boldsymbol{\rho}}$, in turn, admits the exact decomposition:

$$\boldsymbol{B}^{\boldsymbol{\chi}}_{\boldsymbol{\rho}} = \overline{\boldsymbol{B}^{\boldsymbol{\chi}}} + \beta_\rho\widetilde{\boldsymbol{B}^{\boldsymbol{\chi}}}_{0,0} + \alpha_\rho\widetilde{\boldsymbol{B}^{\boldsymbol{\chi}}}_{1,0} - \alpha_\rho\,\widetilde{\boldsymbol{B}^{\boldsymbol{\chi}}}_{1,1} \tag{C.125}$$

with the three-dimensional case convention. Finally:

$$\boldsymbol{K}^r_{\boldsymbol{\rho}} = \overline{\boldsymbol{K}^r} + \beta_\rho\widetilde{\boldsymbol{K}^r}_{(0,0)} + \alpha_\rho\widetilde{\boldsymbol{K}^r}_{(1,0)} - \alpha_\rho\,\widetilde{\boldsymbol{K}^r}_{(1,1)}\,, \tag{C.126}$$

again with the convention of the three-dimensional case.

References

1. J.-L. Auriault, C. Boutin, and C. Geindreau. *Homogenization of Coupled Phenomena in Heterogeneous media*. Wiley, 1996.
2. J.-L. Auriault and J. Lewandowska. Diffusion/adsorption/advection macrotransport in soils. *European Journal of Mechanics*, 15:681–704, 1996.
3. A. Bansoussan, J.-L. Lions, and G. Papanicolaou. *Asymptotic Analysis for Periodic Structures*. AMS chelsea publishing, 1978.
4. K. Bourbatache, O. Millet, A. Aït-Mokhtar, and O. Amiri. Chloride transfer in cement-based materials. Part 1. theoretical basis and modelling. *International Journal For Numerical And Analytical Methods In Geomechanics*, 37:1614–1627, 2013.
5. K. Bourbatache, O. Millet, A. Aït-Mokhtar, and O. Amiri. Chloride transfer in cement-based materials. Part 2. experimental study and numerical simulations. *International Journal For Numerical And Analytical Methods In Geomechanics*, 37:1628–1641, 2013.
6. K. Bourbatache, O. Millet, and C. Moyne. Upscaling diffusion-reaction in porous media. *Acta Mechanica*, 231:2011–203, 2020.
7. M. K. Bourbatache. *Modélisation du transfert des ions chlorure dans les matériaux cimentaires par homogénéisation périodique*. PhD thesis, Université de La Rochelle, 2009.
8. M. K. Bourbatache, T. D. Le, and O. Millet. Limits of classical homogenization procedure for coupled diffusion-heterogeneous reaction processes in porous media. *Transport in Porous Media*, 140:437–457, 2021.
9. M. K. Bourbatache, O. Millet, and K. Aït Mokhtar. Ionic transfer in charged porous media. *International journal of Heat and Mass Transfer*, 55:5979–5991, 2012.
10. M. K. Bourbatache, O. Millet, and K. Aït Mokhtar. Multiscale periodic homogenization if ionic transfer in cementitious materials. *International journal of Heat and Mass Transfer*, 52:1489–1499, 2016.
11. M. K. Bourbatache, O. Millet, and G. Gagneux. Justification of a new original homogenized model for ionic diffusion in porous media. *Journal of Applied Mechanics*, 90, 2023.
12. M. K. Bourbatache, O. Millet, T. D. Le, and C. Moyne. Homogenized model for diffusion and heterogeneous reaction in porous media: Numerical study and validation. *Applied Mathematical Modelling*, 111:486–500, 2022.
13. S. Chaturantabut and D. C. Sorensen. Nonlinear model reduction via discrete empirical interpolation. *Journal of Scientific Computation*, 32:2737–2764, 2010.
14. Q. Chen, C. Xiao, Z. Yang, J. Tabet, and X. Chen. Deep neural network homogenization of multiphysics behavior for periodic piezoelectric composites. *Composites Part A: Applied Science and Manufacturing*, page 108421, 2024.
15. A. Falaize, E. Liberge, and A. Hamdouni. Pod-based reduced order model for flows induced by rigid bodies in forced rotation. *Journal of Fluids and Structures*, 91, 2019.
16. F. Feyel. Multiscale fe2 elastoviscoplastic analysis of composite structures. *Computational Materials Science*, 16:344–354, 1999.
17. L. Fick, Y. Maday, A. T. Patero, and T. Paddei. A reduced basis technique for long-time unsteady turbuent flows. *Journal of Computational Physics*, 2017.
18. F. Fritzen and M. Leuschner. Nonlinear reduced order homogenization of materials including cohesive interfaces. *Computational Mechanics*, 56:131–151, 2015.
19. G. Gagneux and O. Millet. General properties of the nernst-planck-poisson-boltzmann system describing electrocapillary effects in porous media. *Journal of Elasticity*, 117:213–230, 2014.
20. G. Gagneux and O. Millet. A survey on properties of nernst-planck-poisson system. application to cementitious materials. *Applied Mathematical Modelling*, 40:846–858, 2016.
21. N. Gouy. Sur la constitution de la charge électrique à la surface d'un électrolyte. *Journal de la Physique*, IX, 1910.
22. P. Gutierrez-Castillo and B. Thomases. Proper orthogonal decomposition (pod) of the flow dynamics for a viscoelastic fluid in a four-roll mill geometry at the stokes limit. *Journal of Non-Newtonian Fluid Mechanics*, 264:48–61, 2019.
23. N. Lange, G. Hüter, and B. Kiefer. A monolithic hyper rom fe2 method with clustered training at finite deformations. *Computer Methods in Applied Mechanics and Engineering*, 418:116522, 2024.

24. T. Lassila, A. Quarteroni, and G. Rozza. A reduced basis model with parametric coupling for fluid-structure interaction problems. *SIAM Journal on Scientific Computing*, 34:A1187–A1213, 2012.
25. T. D. Le, M. K. Bourbatache, and O. Millet. A spectral approach for homogenization of diffusion and heterogeneous reaction in porous media. *Applied Mathematical Modeling*, 104:666–681, 2022.
26. T. D. Le, C. Moyne, M. K. Bourbatache, and O. Millet. Upscaled model for the diffusion/heterogeneous reaction in porous media: boundary layer problem. *Advances in Water Ressources*, 179:104500, 2023.
27. E. Liberge, M. Pomarede, and A. Hamdouni. Reduced-order modeling by pod-multiphase approach for fluid-structure interaction. *Revue européenne de mécanique numérique*, 19:41–52, 2010.
28. A. Moreau, A. Falaize, C. Allery, and O. Millet. Geometry ependent reduced-order models for the computation of homogenized transfer properties in porous media. *Acta Mechanica*, 232:4429–4459, 2021.
29. C. Moyne and M. A. Murad. A two-scale model for coupled phenomena and onsager's reciprocity relations in expansive clays : I homogenization analysis. *Transport in Porous Media*, 62:333–380, 2006.
30. C. Moyne and M. A. Murad. A two-scale model for coupled phenomena and onsager's reciprocity relations in expansive clays : Ii computational validation. *Transport in Porous Media*, 63:13–56, 2006.
31. M. Oulghelou and C. Allery. Optimal control based on adaptive model reduction approach to control transfer phenomena.
32. M. Oulghelou and C. Allery. A fast and robust sub-optimal control approach using reduced order modes adaptation techniques. *Applied Mathematics and Computation*, 333:416–434, 2018.
33. A. Quarteroni, A. Manzoni, and F. Negri. *Reduced Basis Methods for Partial Differential Equations: An introduction*. Springer, 2016.
34. G. Rozza, D. B. P. Huynh, and A. Manzoni. Reduced basis approximation and a posteriori error estimation for stokes flows in parametrized geometries : roles of the inf-sup stability constants. *Numerische Mathematik*, 125:115–152, 2013.
35. G. Rozza, N. D. Malik, M. Tezzele, M. Girfoglio, S. Giovanni, and A. Mola. Advances in reduced order methods for parametric industrial problems in computational fluid mechanics. In *6th European Conference on Computational Mechanics*, 2018.
36. G. Rytwo. Applying a gouy-chapman-stern model for adsorption of organic cations to soils. *Applied Clay Science*, 24:137–147, 2004.
37. E. Sanchez-Palencia. *Non-Homogeneous Media and Vibration Theory*. Springer, 1980.
38. L. Sirovich. Turbulence and the dynamics of coherent structures. i. coherent structures. *Quarterly of applied mathematics*, 45:561–571, 1987.
39. L. Sirovich. Turbulence and the dynamics of coherent structures part i : coherent structures. *Quarterly of Applied Mathematics*, XLV:561–571, 1987.
40. C. Stemelen, D. abd Moyne and T. Lemaire. Modelling of electro-osmosis in clayery materials including PH effects. *Physics abd Chelistry of the Earth*, 31:441–452, 2007.
41. S. Whitaker. Simultaneous heat, mass and momentum transfer in porous media : A theory of drying. *Advances in Heat Transfer*, 13:119–203, 1977.
42. S. Whitaker. A simple geometrical derivation of the spatial averaging theorem. *Chemical Engineering Science*, 19:50–52, 1985.
43. D. Xiao, F. Fang, A. G. Buchan, C. C. Pain, I. M. Navon, J. Du, and G. Hu. Non-linear model reduction for the navier-stokes equations using residual deim method. *Journal of Compuational Physics*, 263:1–18, 2013.
44. J. Yvonnet and Q.-C. He. The reduced model multiscale method (r3m) for the non-linear homogenization of hyperelastic media at finite strains. *Journal of Computational Physics*, 223:341–368, 2007.
45. J. Yvonnet, Q.-C. He, and P. Li. Reducing internal variables and improving efficiency in data-driven modelling of anisotropic damage from rve simulations. *Computational Mechanics*, 72:37–55, 2023.